NASA Technical Memorandum 108491

Bearing Defect Signature Analysis Using Advanced Nonlinear Signal Analysis in a Controlled Environment

CDDF Final Report, Project No. 93-10

T. Zoladz, E. Earhart, and T. Fiorucci
Marshall Space Flight Center • MSFC, Alabama

National Aeronautics and Space Administration
Marshall Space Flight Center • MSFC, Alabama 35812

May 1995

TABLE OF CONTENTS

LIST OF ILLUSTRATIONS

LIST OF ILLUSTRATIONS (Continued)

LIST OF ILLUSTRATIONS (Continued)

LIST OF ILLUSTRATIONS (Continued)

LIST OF ILLUSTRATIONS (Continued)

LIST OF ILLUSTRATIONS (Continued)

ABBREVIATIONS AND ACRONYMS

A/D	analog-to-digital
ABC	autobicoherence
ABS	autobispectrum
AE	acoustic emission
ATD	alternate design (SSME)
BS	ball spin frequency (Hz)
C	roller/ball train cage frequency (Hz)
CDDF	Center Director's Discretionary Fund
HPOTP	high pressure oxygen turbopump (SSME)
IRIG	Inter-Range Instrumentation Group
IRP	inner race defect passing frequency (Hz)
N	rotor synchronous speed (Hz)
PSD	power spectral density
RPM	rounds per minute
RS	rolling element spin frequency (Hz)
SSME	space shuttle main engine
T_N	fundamental period of rotor shaft rotation (s)

TECHNICAL MEMORANDUM

BEARING DEFECT SIGNATURE ANALYSIS USING ADVANCED NONLINEAR SIGNAL ANALYSIS IN A CONTROLLED ENVIRONMENT CDDF FINAL REPORT (NO. 93-10)

I. INTRODUCTION

Accurate machinery fault detection and diagnosis have always been significant technical challenges in the aeronautics and transportation industries. Within the aerospace industry, the reliable health monitoring of propulsion systems is a necessity in preventing catastrophic system failures and costly engine down time due to false alarms. Since machines "talk" through their sounds and vibrations, an analyst, given the appropriate set of tools, can listen to their complaints and diagnose their ailments. The signs and symptoms of these ailments appear as subtle complex dynamic signatures hidden deep within random signals sensed through high-frequency instrumentation mounted externally to the machine. However, these symptoms are often confused with other responses emitted by the monitored machine such as rotor dynamic, structural, and environmental operational elements, along with electronic line noise contributed by the sensor signal conditioning equipment. Ultimately, the success of a machinery fault detection and isolation program relies on its ability to first extract these complex dynamic signals from random data, then to form an accurate interpretation and diagnosis consistent with these "complaints" from the machine.

During the development of the space shuttle main engine (SSME), significant progress has been made within both NASA and the aerospace communities toward improving the machinery fault diagnostic function through research in instrumentation, modeling, and dynamic signal analysis. This research has significantly enhanced the safety of space shuttle operations. Within the Structures and Dynamics Laboratory of Marshall Space Flight Center, major progress has been made through the development of a hierarchy of advanced nonlinear signal spectral analysis techniques for mechanical signature analysis. The research has progressively led to the introduction of new signal processing techniques which can identify intelligent machine operating state information hidden deep within the extraneous corruptive noise of dynamic measurements, information often unidentifiable using conventional signal analysis methods. By providing additional insight into the monitored system response, these "tools" allow better identification of well-hidden defect symptoms such as bearing flaws within SSME high-speed turbopumps. Moreover, by using phase information inherent in these signals, the nonlinear analysis methods separate false-alarm, i.e., benign, signatures from true defect signals allowing hardware integrity to be maintained.

This document summarizes a Center Director's Discretionary Fund (CDDF) research effort that investigated rolling element bearing fault dynamic signatures. The sponsored research used both traditional and state-of-the art (acoustic emission (AE)) sensors and signal-processing techniques in the characterization of high-frequency data from a laboratory rotor system seeded with bearing faults. The research concentrated on applying nonlinear signal analysis techniques which identify hidden relationships between multiple spectral components within and across high-frequency monitoring channels in diagnosing implanted bearing faults. The coupling of these nonlinear signal analysis "tools" with AE sensor technology was the innovative focus of this research.

II. TEST SETUP

This research effort utilized a highly instrumented rotor assembly as a test article (fig. 1). Since the commercially available rotor rig was not fitted with off-the-shelf rolling element bearings, it was modified with a dual bearing block which allowed for quick bearing change-out to expedite the bearing defect data gathering and analysis process. Due to this bearing retrofit process, a rotor dynamic analysis was performed on the assembly to determine if any rotor modes would interfere with the bearing defect analysis. The analysis concluded that no rotor modes would be excited in the operating range of the assembly (0 to 10,000 r/min) during testing.

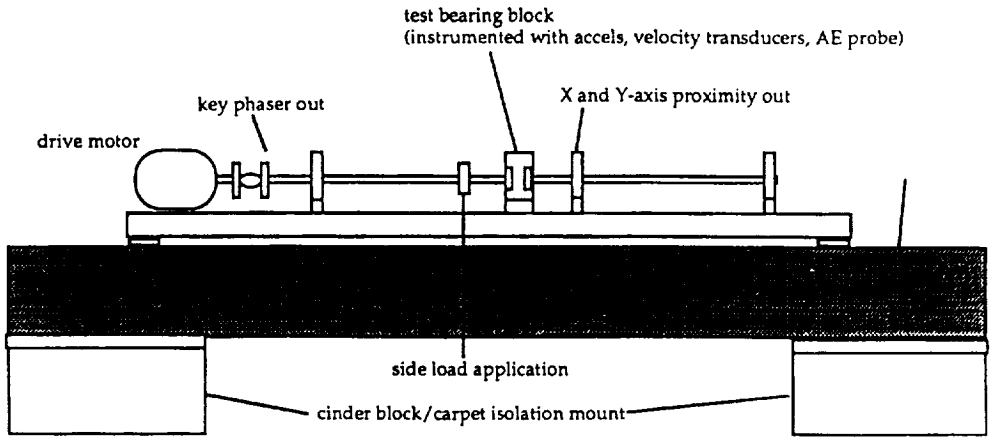

Figure 1. Rotor assembly test article for CDDF-sponsored research.

In this study, both ball and roller type rolling element bearings were tested. An 8-ball, deep-groove, ball bearing manufactured by SKF, model number 6202 JEM, and an 11-roller cylindrical roller bearing also manufactured by SKF, model number NU 202 ECP, were chosen as test articles for the research. The appendix contains calculations for the characteristic bearing frequencies, as ratios to rotor speed, for the two test bearings. These frequencies, which include cage (ball/roller train), outer rolling element passing, inner rolling element passing, and rolling element spin, are calculated using simple well-documented formulas which are a function of ball/roller diameter, pitch diameter, rolling element contact angle, and number of rolling elements.[1]

Conventional vibration sensors including accelerometers, velocity probes, and proximitors were mounted at various locations on the rotor/bearing block assembly. Along with these traditional high-frequency sensors, one AE probe was affixed to the test bearing block during all testing. Use of AE technology for bearing defect analysis is comparatively recent.[2] Use of an AE type sensor in bearing fault detection is very promising since it provides immunity from structural, rotor dynamic, and environmental noise that floods conventional sensors. Use of the AE sensor allows subsequent analysis to focus on the bearing condition. AE sensors are designed to detect energy traveling as Lamb waves from defect source to sensor, with the wave front passing through the structure at its shear wave velocity. It is the elastic propagation of these waves in the material media that constitutes the AE energy/signals. These bursts of emissions are typically sensed in the 100- to 1,000-kHz region.[3] These AE sensor response regions typically extend much higher in frequency than conventional mechanical signature analysis bandwidths using traditional transducers, i.e., accelerometers, which seldom exceed 20 kHz. However, along with the expected benefits associated with the AE sensor's higher-frequency response come challenging analog-to-digital (A/D)

conversion requirements. In this CDDF analysis, a Physical Acoustics Corp. model S9208 AE sensor was used to collect emissions from the bearing test articles through the bearing support block. Since the AE probe had broadband sensitivity extending out past 1.25 MHz, the channel was recorded in a direct recording mode in parallel with the remaining conventional sensor channels in a frequency modulating (FM) recording mode. Direct mode recording of the AE channel allowed for an analog recording bandwidth of 400 Hz to 2 MHz, while the FM channels captured signal input in the range from 0 Hz to 40 kHz. This FM mode was sufficient for the conventional lower-frequency response accelerometers, velocity probes, and proximitors. Due to its high-frequency response, the AE channel was digitized separately during A/D processing. In fact, in order for the existing laboratory A/D system to successfully sample and log the acquired data, the replay tape speed of the analog recorder had to be reduced from 120 to 3.75 in/s, a factor of 32. In order to synchronize the AE data with the conventional low-frequency data recorded on the FM channels, an IRIG time code signal was concurrently digitized with all sensor data.

As previously mentioned, both roller and ball type rolling element bearings were used as test articles during the investigation. In an effort to simulate early spalling damage, single-point seeded faults were implanted in the bearings in the form of fine linear axial (relative rotor shaft) scratches in the rolling elements themselves and their raceways. The bearings were then mounted on sleeves, affixed to the rotor shaft, and placed into the bearing block with contact between the bearing outer races and the block preventing rotation of their outer raceways. Several bearing defect scenarios were tested during this CDDF study, however, only three are presented in this report:

- Single-roller type bearing with no imbedded faults
- Single-roller type bearing with small axially extending scratch imbedded in inner raceway
- Single-roller type bearing with small axially extending scratch imbedded in one rolling element.

During each of the bearing tests, rotor speed was linearly increased from idle to 10,050 r/min (168 Hz) where it dwelled for several seconds and then returned back to idle. Typically, test durations were approximately 140 s. During testing, selected data channels were monitored on dynamic signal analyzers and oscilloscope for test control.

III. BEARING FAULT PATTERNS AND ANALYSIS METHODS

A. Bearing Fault Patterns

Faults in bearings tend to generate characteristic frequencies which can be invaluable in diagnosing their health. Even though the computation of fundamental characteristic bearing frequencies is straightforward, other factors such as modulation effects can complicate the bearing defect vibration signature. McFadden and Smith[4,5] give an excellent discussion of the vibration signatures produced by both single- and multiple-point defects within rolling element bearings. In their analytic model, the sensed bearing defect vibration waveform is primarily determined by bearing geometry (which allows for calculation of impact rates), bearing load distribution, and the transmission characteristics of the bearing defect energy from the point of impact to the sensing location. Figure 2 shows the general form of the analytically predicted envelope spectrum for the vibration emitted by a bearing with a single-point defect.

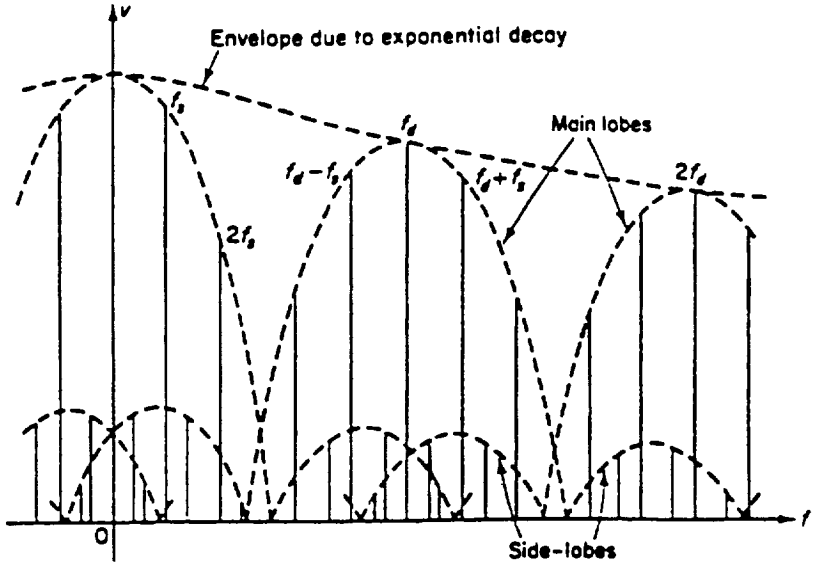

Figure 2. Analytically predicted bearing defect vibration spectrum.[4 5]

The term envelope indicates that the spectrum was recovered using a high-frequency resonance, also referred to as envelope detection, technique. If the periodic impacts generated by a defective bearing surface making contact with another bearing surface excite, i.e., "ring," high-frequency bearing/machine structural or transducer resonances, the character of the bearing vibration can be recovered from the excited resonant band of energy. Of interest in envelope analysis is not what system or transducer resonance is excited (the carrier), but the impulse repetition frequency (the envelope) which allows characterization of the bearing fault. Given optimal transmissibility between source and sensor in the frequency band containing the characteristic bearing frequencies themselves, the spectral pattern shown in figure 2 could be recovered using conventional signal analysis techniques without envelope-type analysis. However, in real-life machinery monitoring situations, these bearing defect components are frequently highly damped since they are sensed externally on the machine housing. Moreover, if they are apparent in the low-frequency region of the vibration signal, they are commonly confused with other rotor dynamic, hydrodynamic, and environmental noise sources that tend to confound the signal spectrum. In this CDDF study, nonlinear spectral analysis was applied to such confusing multiple source signals to determine if bearing defect signatures could be separated from unrelated "noise" without relying on envelope detection processing. Later, these results were compared to envelope spectral analysis results using both accelerometer and AE-sensed signals. Finally, nonlinear spectral analysis was applied to recovered envelope signals to further enhance bearing defect signature retrieval results and to verify the analytically predicted nonlinear complex modulation sideband structures shown in figure 2.

As previously mentioned, bearing defect vibration character is dictated by bearing geometry, bearing load, and defect energy transmission characteristics. The analytic bearing fault pattern of figure 2 consists of clusters or groups of discrete frequencies with members in each successive group separated by a frequency represented by "f_s," the modulating frequency, and the center-most peak of each group spaced in frequency by "f_d," the carrier frequency. A bearing with a single inner race defect would exhibit a modulating frequency equal to shaft rotational speed and a carrier frequency corresponding to its inner race element passing frequency. On the other hand, a bearing with a single rolling element defect would exhibit a modulating frequency equivalent to its cage rotational frequency and a carrier frequency of rolling element spin frequency. The lobing character seen in the progressive groups of spectral components in figure 2 is due to the bearing load cycle which

influences the bearing surface impact intensity. The largest component in each of the successive clusters is the element passing or spin frequency. The general decay in amplitude of the successive groups of frequencies is attributed to the damping of the defect impulses during wave propagation from source to sensor.

B. Analysis Methods

1. Conventional Power Spectral Density Analysis. Conventional bearing diagnostic evaluation is done by assessing the power spectral density (PSD) content of monitored high-frequency bearing/machine instrumentation channels. Baseline response, i.e., PSD amplitude levels, at characteristic bearing frequencies for given machine instrumentation locations are developed and archived for trend analysis with newly acquired data. Such analysis is beneficial to a machinery health monitoring program but can be somewhat limited as a bearing health diagnostic tool in several instances. For instance, in several machinery systems, externally sensed bearing vibrations are highly damped, and, by the time bearing characteristic frequencies are sensed on the machine housing, significant bearing degradation has already occurred. In other instances, complex spectral content due to machinery rotor dynamic, hydrodynamic, or environmental responses resembles the bearing frequencies (fault patterns) being monitored and confuses the bearing health diagnosis. The biggest shortcoming with linear spectral analysis anchored bearing health analysis is its oversight of pertinent intra- and cross-channel phase relationships existing between the many spectral components associated with complex bearing vibration waveforms. This limitation of the conventional PSD analysis is what motivated the development of several advanced nonlinear signal analysis tools within the Structures and Dynamics Laboratory over the past decade for propulsion system turbomachinery analysis.

2. Nonlinear/Bispectral Analysis. Nonlinear spectral analysis techniques improve bearing vibration signature analysis by exploiting hidden nonlinear phase relationships within the spectra of acquired high-frequency diagnostic data.[6–8] As seen in the complex defective bearing spectrum shown in figure 2, fundamental bearing signatures consist of key harmonic and modulation sideband structures. However, these patterns are not always easily identifiable. Where PSD analysis relies only on identification of the frequency spacings in such patterns, nonlinear analysis identifies the inherent phase coupling existing between individual members of such complex frequency structures.

As the PSD function is a second moment statistic of a random signal, the auto-bispectrum (ABS) represents the third joint moment among three different waves, spectral components, at frequencies ω_1, ω_2, and the sum frequency $\omega_1+\omega_2$, and can be estimated by:

$$B_{xxx}(\omega_1,\omega_2) = E[X(\omega_1)X(\omega_2)X^*(\omega_1+\omega_2)] \quad , \tag{1}$$

where $X(\omega)$ is the Fourier transform of the monitored instrumentation channel, $x(t)$. The auto-bicoherence (ABC), a normalized bispectrum, is defined as:

$$b^2_{xxx}(\omega_1,\omega_2) = \frac{|B_{xxx}(\omega_1,\omega_2)|^2}{E[|X(\omega_1)X(\omega_2)|^2]E[|X(\omega_1+\omega_2)|^2]} \quad . \tag{2}$$

The ABS $B_{xxx}(\omega_1,\omega_2)$ is a function of two independent frequencies, ω_1 and ω_2 (along with an implicit third wave of frequency $\omega_1+\omega_2$), rather than a single-frequency argument as with a PSD. Therefore, a

three-dimensional figure would be required to display a bispectrum since it is a function of two frequency arguments. However, to maximize the visualization effect, one of the bi-frequency arguments, ω_1, can be fixed at some particular frequency of interest, such as a bearing characteristic frequency, while the other frequency argument, ω_2 , sweeps through the entire analysis frequency range of the input signal.

Analytically, auto/cross bicoherence can be shown bounded by zero and unity. Since basic bearing defect mechanisms produce amplitude modulated vibrations involving three basic spectral components at frequencies ω_1, ω_2, and their sum frequency, $\omega_1+\omega_2$, bicoherence is a perfect candidate for bearing diagnostic applications. Even though a simple PSD might be able to identify the power distribution at these three particular bearing-related frequencies, the existence of modulation can only be proven by identifying/extracting the coherent phase relationship among the three frequency components. The phase information of the bispectrum in equation (1) provides a unique tool for identifying such phase coupling. If the wave at frequency $\omega_1+\omega_2$, is perfectly correlated to the waves at frequencies ω_1 and ω_2 due to some nonlinear process, then a constant relative phase relationship would exist and can be identified in the bispectral estimation, and, as a result, the associated bicoherence will be equal to one. On the other hand, if the waves at frequency ω_1, ω_2, and $\omega_1+\omega_2$, are totally independent of each other, then the phase of the bispectrum will remain random, and the resulting bicoherence estimation will be reduced to zero.

3. Envelope Detection Analysis. The envelope detection method for bearing fault detection is based on the observation that a bearing characteristic impact frequency (e.g., the rate of inner race element passing) may modulate a bearing/machine structural or sensor resonant frequency. This impacting will ring the particular resonant response at the characteristic repetition rate, or the modulating frequency. Frequently, the harmonics of such bearing impact excitations extend well into the high-frequency region (10 to 100 kHz) to excite the structural or sensor resonant frequencies. The resonant response of the monitored channel is then isolated and referred to as the carrier frequency. However, what is of interest in the bearing analysis is not the carrier frequency, but, rather, the modulating frequency of the carrier, or impact repetition rate. Demodulation of the resonant signals (isolated through appropriate bandpass filtering) through use of a recovery algorithm such as the Hilbert transform[9] method retrieves the instantaneous envelope signals. Subsequent spectral analysis of the recovered envelope, i.e., postenvelope analysis, displays the complex frequency pattern related to the source bearing defect. Unlike the conventional vibration spectrum, the envelope spectrum is void of rotor dynamic, hydrodynamic, and other sources of "noise" which tend to mask the defect. This filtering of extraneous "noise" from pertinent distress signal content is accomplished through focusing analysis on variations in envelope intensity and not through the instantaneous signal intensity.

In this CDDF research, envelope analysis was applied to high-frequency data acquired from both accelerometers and a single AE sensor. Envelope analysis using AE sensed input, although more challenging in terms of digital acquisition and signal processing capability, offers several potential advantages over the more traditional vibration sensing accelerometers. Since AE sensors have extremely high-frequency response ranges (typically 200 kHz to 1.0 MHz), all conventional low-frequency mechanical, hydrodynamic, and environmental responses along with electronic line noise contributions are eliminated. Subsequent envelope analysis is thus allowed to focus on bearing impact related energy which is captured at the AE sensor. Moreover, AE sensors are designed to sense surface (Lamb) waves, which allows for better defect characterization at greater distances from the impact source.

4. Postenvelope Bispectral Analysis. Through this CDDF-sponsored research, a unique technological advancement opportunity relating to bearing defect analysis was made available, i.e., the coupling of nonlinear bispectral signal analysis with AE-acquired bearing signatures recovered from envelope analysis. The central innovativeness of this coupling of signal processing technologies would be in its ability to effectively extract bearing fault patterns from the ultra-high-frequency AE's. Success in this research would justify future efforts in applying the technology to more complex machinery systems such as rocket engine high speed turbopumps. Hopefully, the postenvelope application of nonlinear signal analysis to the AE-recovered bearing vibrations would increase bearing fault detectability and allow identification of faults during their incipient stages.

In this CDDF research, bispectral analysis was successfully applied to AE-sensed bearing signatures in a postenvelope mode, i.e., the nonlinear analysis was applied to recovered envelope signals. Results were compared to those from conventional PSD analysis of low-frequency channels (<5 kHz), bispectral analysis of low-frequency channels, and finally with bispectral analysis of postenvelope accelerometer acquired bearing signatures.

IV. ANALYSIS RESULTS

In this section, the analysis results from three of the bearing defect tests performed during this CDDF-sponsored research will be summarized. Several spectral and temporal data plots are referenced extensively in describing research findings. Results from bearing defect signature recovery efforts for the following three bearing conditions will be discussed:

- Single-roller type bearing with no imbedded faults
- Single-roller type bearing with single axially extending scratch imbedded in inner raceway
- Single-roller type bearing with single axially extending scratch imbedded in one rolling element.

A. Conventional PSD Analysis Results

In this research, the analysis bandwidth used in the conventional PSD analysis was 0 to 5 kHz since the frequency range effectively encompassed all expected characteristic bearing frequencies and modulation sideband families. Figure 3 is a compilation of 0- to 5-kHz PSD's computed from the instantaneous signals acquired from two bearing block accelerometers for the three bearing conditions of no imbedded flaw (figs. 3(a) and 3(d)), imbedded inner race defect (figs. 3(b) and 3(e)), and imbedded rolling element defect (figs. 3(c) and 3(f)). As can be seen in the PSD's, all spectra, including those from the clean bearing test, contain a multitude of frequency components which makes identification of bearing defect signatures very challenging. Using best estimates of the characteristic roller bearing frequencies (appendix), an attempt was made to identify analytically predicted bearing defect vibration patterns as developed in figure 2. For the roller bearing inner race defect case (figs. 3(b). and 3(e)), definite families of sidebands (sum and difference frequencies) spaced by synchronous (rotor) speed, N, centered around harmonics of the predicted inner race defect passing frequency (IRP) can be identified. In an effort to help display this structure in figure 3(b), a template has been superimposed on top of the PSD. Each IRP multiple is identified as an integer with two synchronous-spaced intervals extending to either side. As can be seen in figures 3(b) and 3(e), the first family of synchronous sidebands centered around the fundamental

inner race defect passing frequency, IRP, is very much indistinguishable in the 0- to 5-kHz PSD's of the two accelerometers. Also, the analytically predicted lobing character of the families of synchronous dependent sidebands related to the bearing load cycle is not obvious. For the roller bearing rolling element defect case (figs. 3(c) and 3(f)), neither the predicted fundamental rolling element spin frequency (RS), nor subsequent harmonics are visible in the conventional vibration spectra. In fact, when comparing roller defect case PSD's of figures 3(c) and 3(f) to the clean bearing PSD's of figures 3(a) and 3(d), the defective bearing spectra contain far fewer discrete components, i.e., far fewer candidates for bearing frequencies. However, subsequent postenvelope analysis provides more insight into the rolling element defect test case.

Figure 4 shows sample instantaneous acceleration waveforms over roughly 20 cycles of shaft rotation (120-ms duration) which coincide with the PSD's of figure 3. The low-frequency (0- to 5-kHz) waveforms are dominated by rotor dynamic synchronous/synchronous harmonic reposes. No evidence of impact type events related to the imbedded bearing flaws can be seen in these low-frequency characterizations.

B. Nonlinear/Bispectral Analysis Results, 0- to 5-kHz Data

In an attempt to better extract and confirm complex bearing defect patterns in the conventional low-frequency bearing spectra, nonlinear spectral analysis was applied. Specifically, bicoherence spectra were generated for the defective bearing test cases in an attempt to identify key harmonic and modulation sideband signal structures predicted analytically (fig. 2). Figure 5(b) shows the bicoherence estimation for the inner race defect test case with a bispectral reference frequency corresponding to the predicted roller inner race passing rate. In actuality, a tricoherence[6,7] estimation with the first reference frequency set to zero, equivalent to a bicoherence estimation, was made. In this case, bispectral analysis successfully identifies the complex modulation sideband families seen in the corresponding PSD shown in figure 5(a). The bispectral analysis accomplishes this characterization of the vibration data by identifying key nonlinear phase couplings between individual members of the families of bearing frequencies. Similar analysis was also applied to high-frequency data from the rolling element defect test. Figure 6(b) shows the bicoherence estimation for the rolling element defect test case with the reference frequency set at the predicted roller spin frequency for the test bearing. In the figure, no significant bicoherence peaks identifying nonlinear coupling between predicted bearing frequencies are apparent. In other words, unlike subsequent postenvelope analysis, bispectral analysis of conventional vibration data was unsuccessful in diagnosing the bearing defect. Apparently the roller defect vibration signature was much more subtle than originally anticipated.

C. Envelope Detection Analysis Results (Accelerometer Data)

Following the application of conventional PSD and nonlinear bispectral analysis to each bearing test data set, envelope analysis of high-frequency accelerometer (10- to 80-kHz) and AE (50- to 400-kHz) data was performed. For data from both types of transducers, the Hilbert transform method was used in recovering the envelope of the acquired original wideband instantaneous waveforms. Once recovered, the envelope signals, which are themselves instantaneous waveforms of the envelopes of the original time signals, were subsampled to provide analysis bandwidths (of the order) consistent with the conventional PSD and bispectral analyses previously discussed.

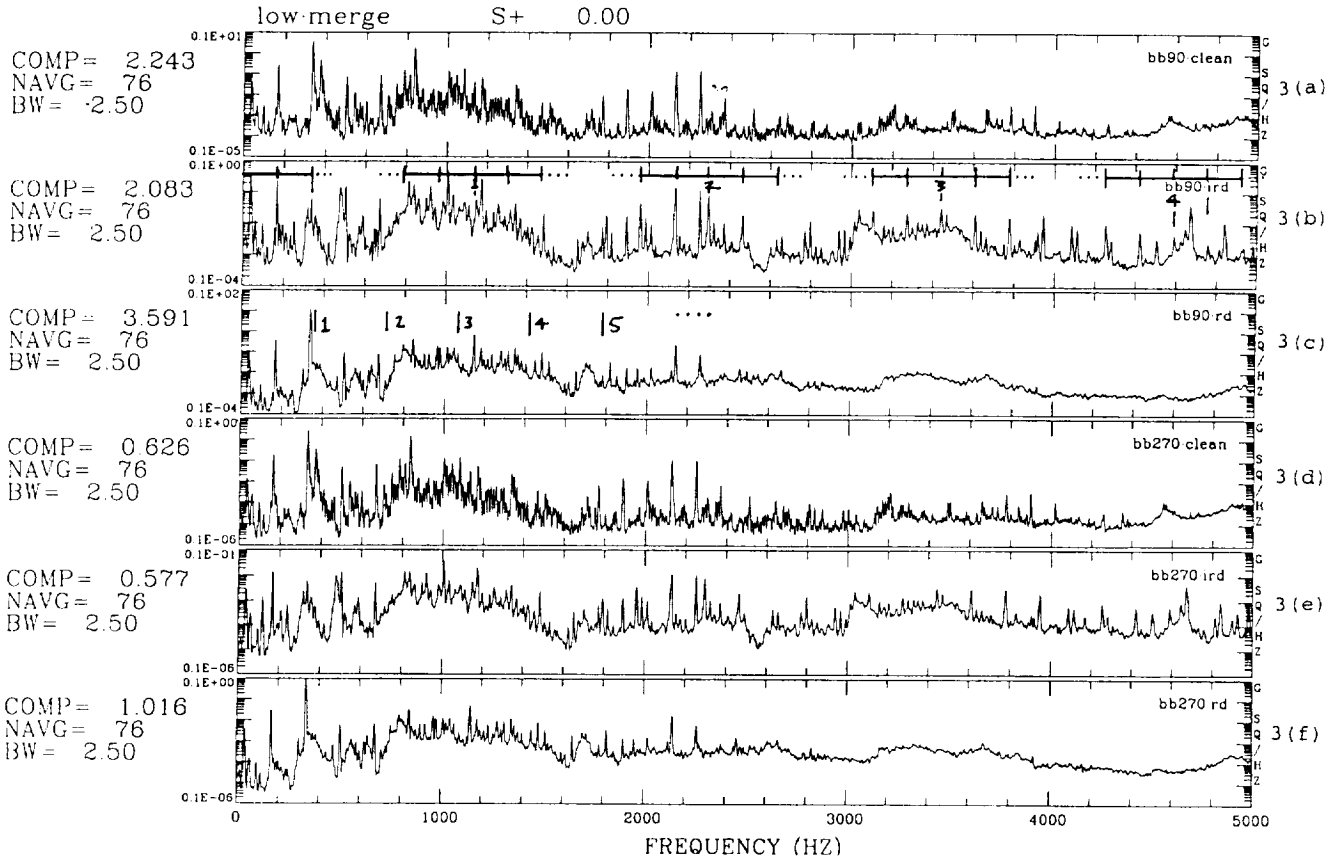

3(a). Bearing block 90° location accelerometer spectrum for good roller bearing.

3(b). Bearing block 90° location accelerometer spectrum for roller bearing with inner race defect.

3(c). Bearing block 90° location accelerometer spectrum for roller bearing with rolling element defect.

3(d). Bearing block 270° location accelerometer spectrum for good roller bearing.

3(e). Bearing block 270° location accelerometer spectrum for roller bearing with inner race defect.

3(f). Bearing block 270° location accelerometer spectrum for roller bearing with rolling element defect.

Figure 3. Conventional 5-kHz acceleration spectra across several test bearing configurations.

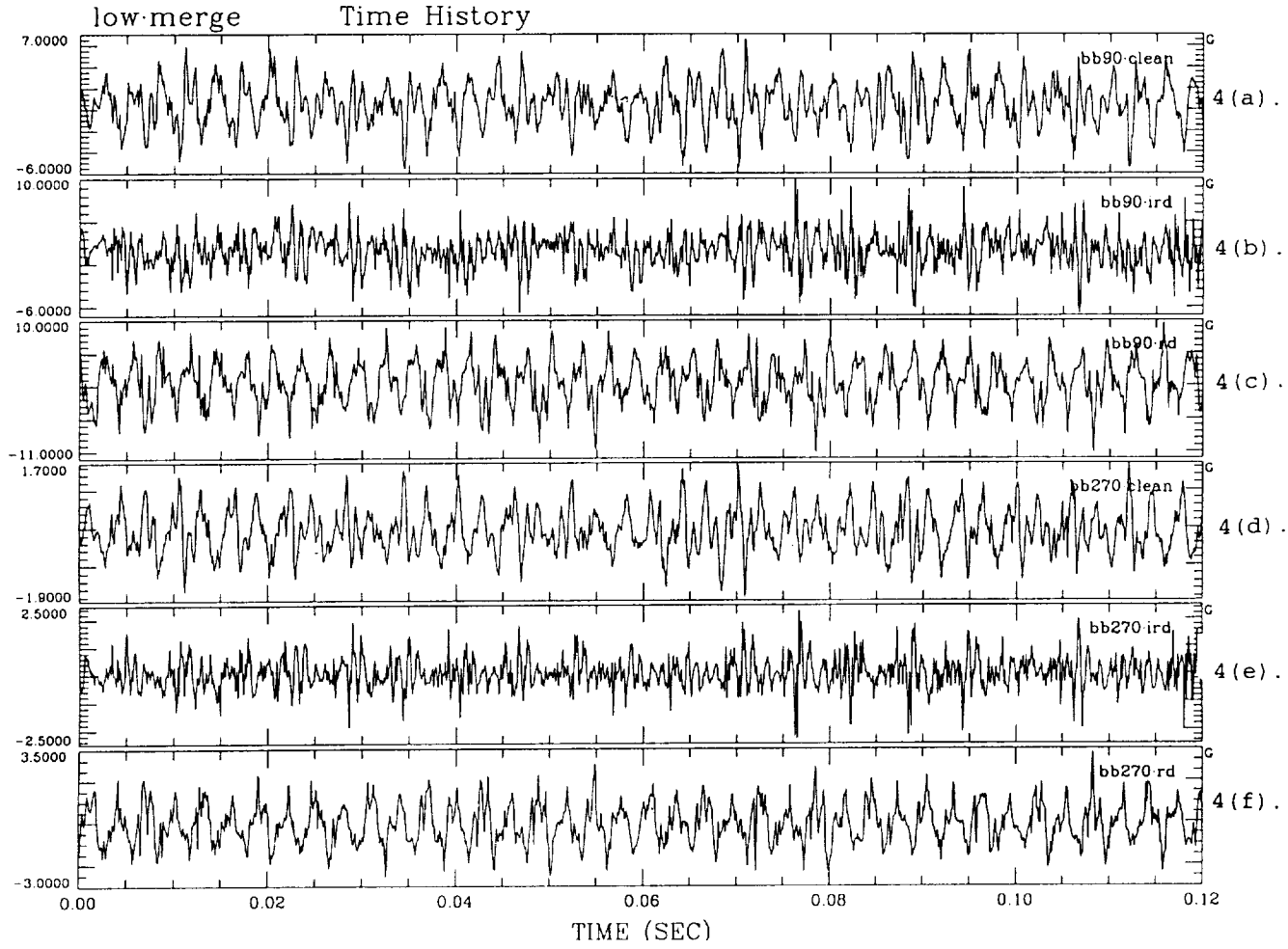

4(a). Bearing block 90° location accelerometer waveform for good roller bearing.

4(b). Bearing block 90° location accelerometer waveform for roller bearing with inner race defect.

4(c). Bearing block 90° location accelerometer waveform for roller bearing with rolling element defect.

4(d). Bearing block 270° location accelerometer waveform for good roller bearing.

4(e). Bearing block 270° location accelerometer waveform for roller bearing with inner race defect.

4(f). Bearing block 270° location accelerometer waveform for roller bearing with rolling element defect.

Figure 4. Raw acceleration (0- to 5-kHz band limited) waveforms across several test bearing configurations.

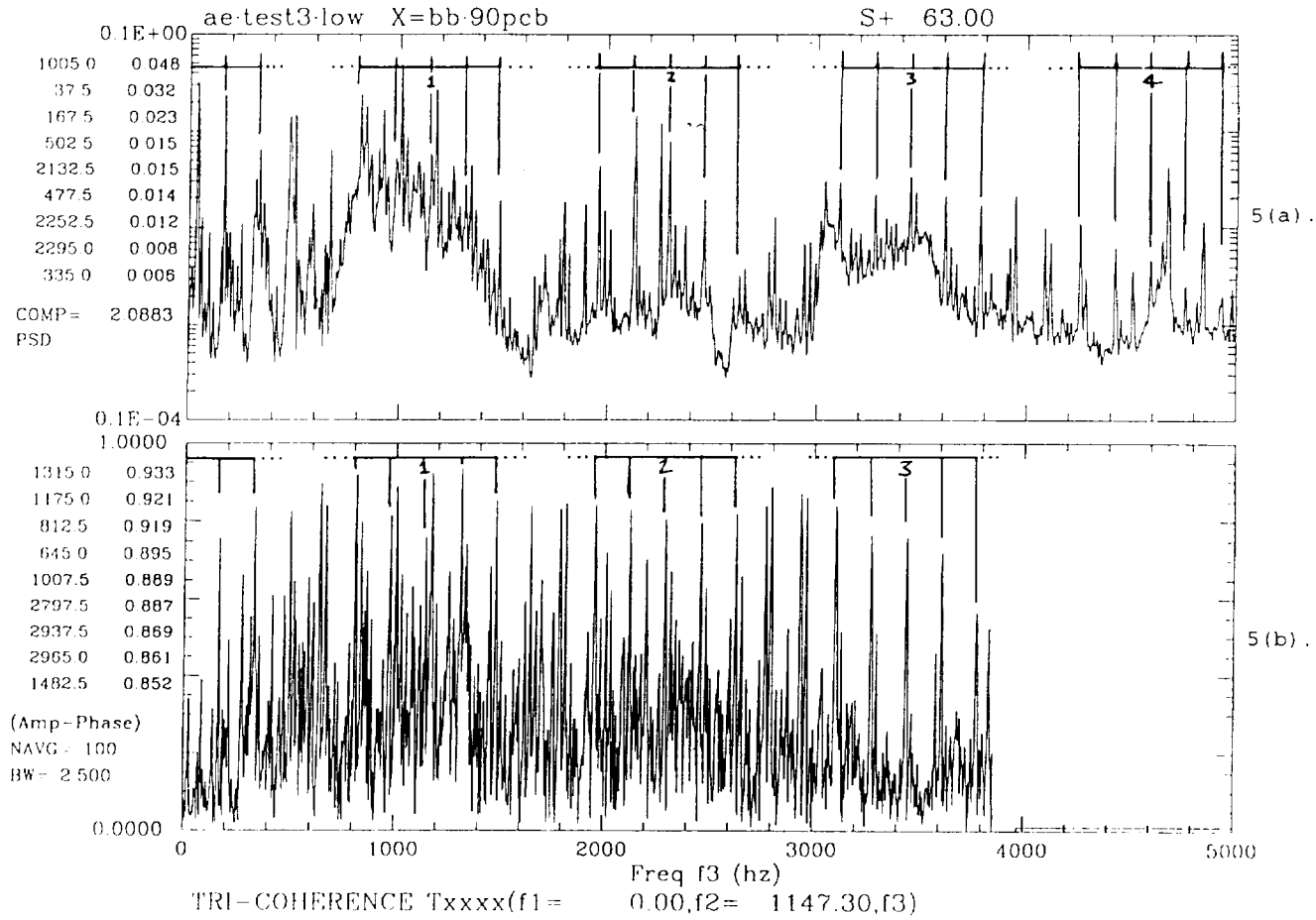

5(a). 0- to 5-kHz PSD for bearing block 90° location accelerometer.

5(b). 0- to 5-kHz bicoherence spectrum corresponding to PSD of figure 5(a), reference frequency set at inner race roller passing impact rate.

Figure 5. Roller bearing inner race defect bicoherence estimation using bearing block 90° location accelerometer data (0 to 5 kHz) for a reference frequency set at inner race roller passing impact rate.

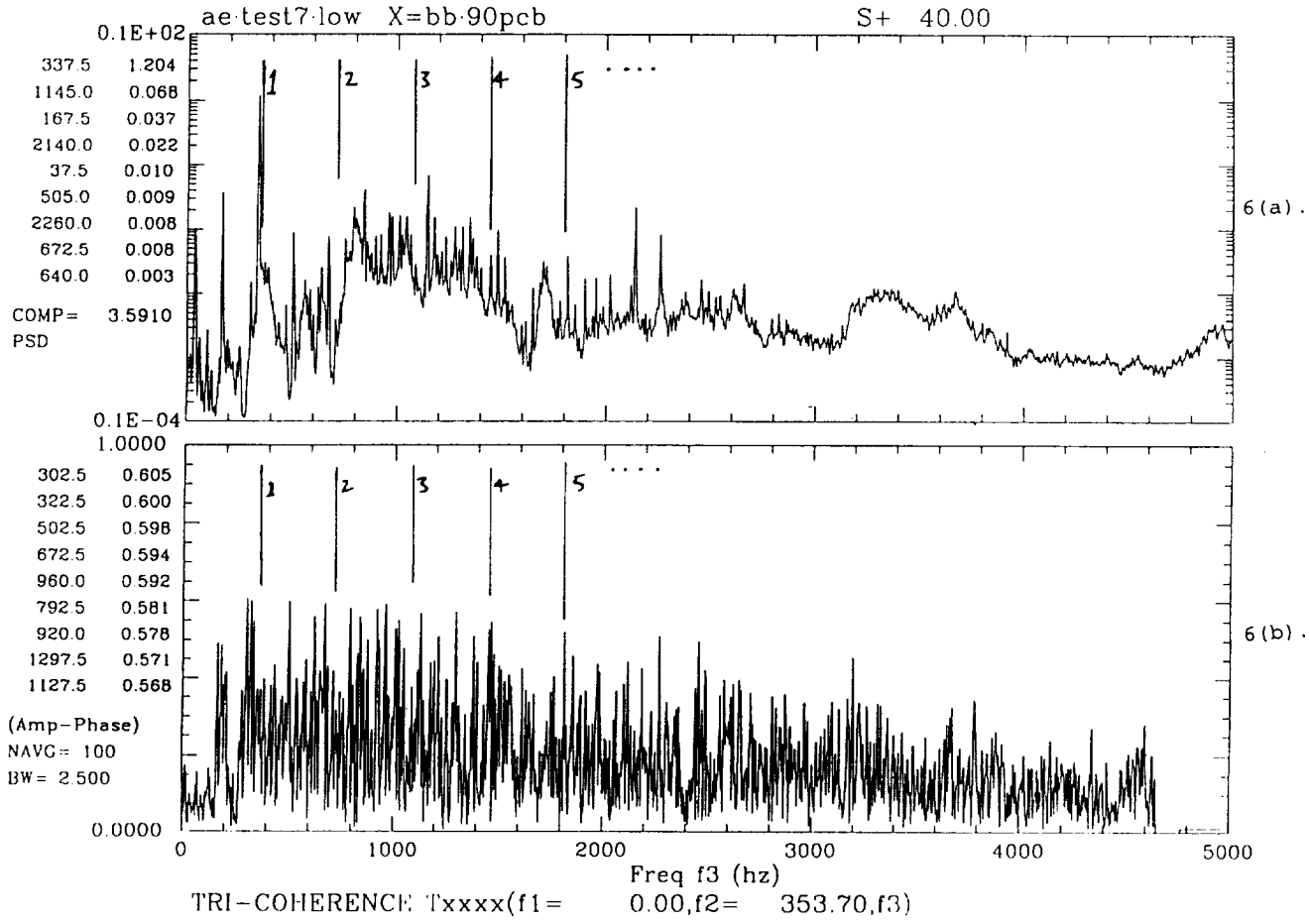

6(a). 0- to 5-kHz PSD for bearing block 90° location accelerometer.

6(b). 0- to 5-kHz bicoherence spectrum corresponding to PSD of figure 6(a), reference frequency set at rolling element spin frequency.

Figure 6. Roller bearing rolling element defect bicoherence estimation using bearing block 90° location accelerometer data (0 to 5 kHz) for a reference frequency set at rolling element spin frequency.

Figure 7 is a compilation of PSD's (0 to 130 kHz), computed from the original time signals, used to characterize the wideband responses of the bearing block accelerometers recorded during the testing. As can be seen in the PSD's, no prominent distinguishing features separate the responses of the clean bearing test (figs. 7(a) and 7(d)), the inner race defect test (figs. 7(b) and 7(e)), and the defective rolling element test (figs. 7(c) and 7(f)). Bandpass filtering of the time signals with a passband setting of 10 to 80 kHz was applied to all wideband bearing block accelerometer data prior to envelope analysis. This passband is denoted by the arrows in figure 7(a). Figure 8 shows the set of envelope spectra, i.e., PSD's, recovered from the envelope of the wideband bearing block accelerometer signals. This sequence of PSD's (of the envelope signals) in figure 8 is consistent with the conventional PSD sequence of figure 3 in terms of bearing defect and accelerometer location.

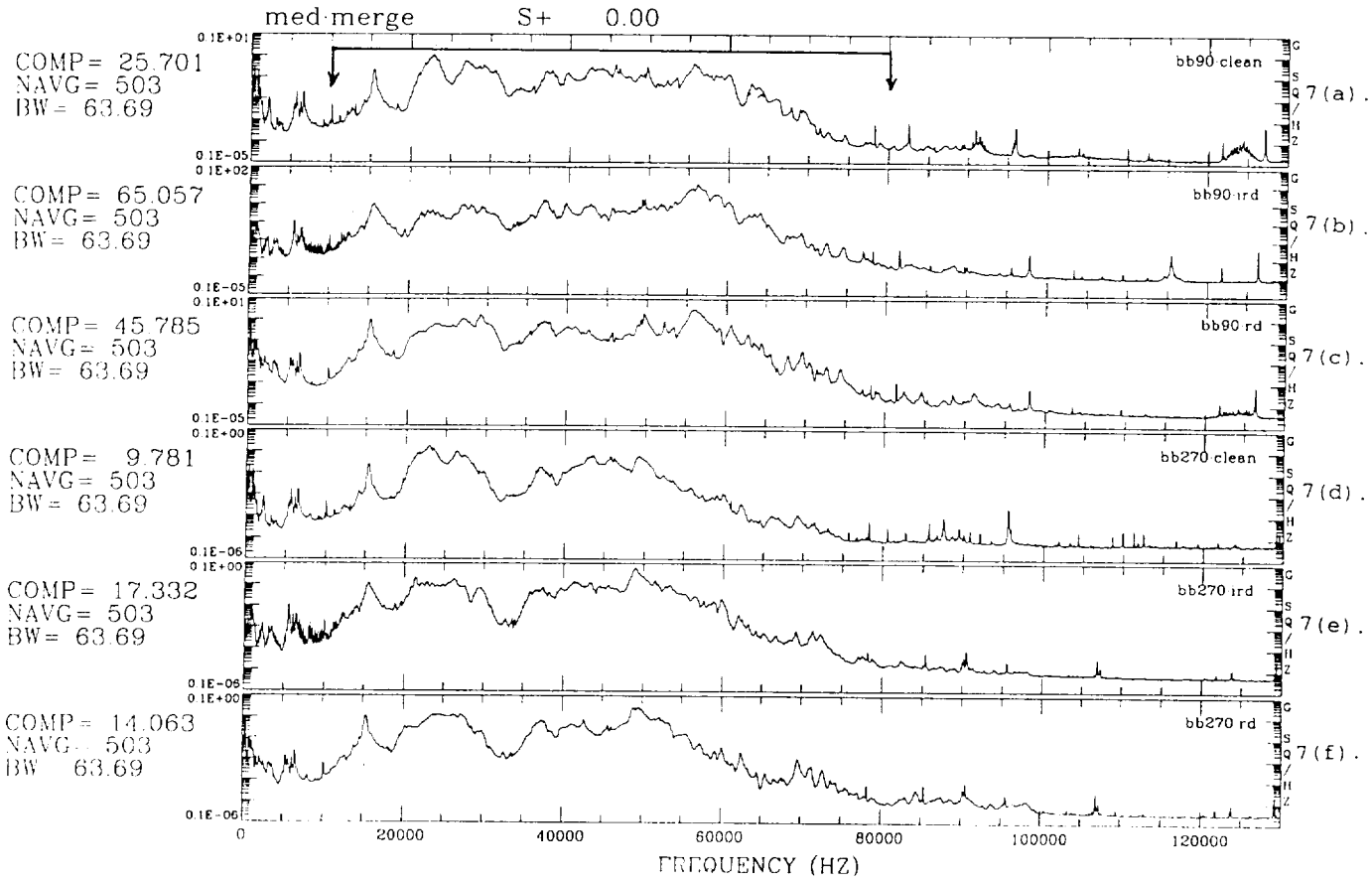

7(a). Bearing block 90° location accelerometer spectrum for good roller bearing.

7(b). Bearing block 90° location accelerometer spectrum for roller bearing with inner race defect.

7(c). Bearing block 90° location accelerometer spectrum for roller bearing with rolling element defect.

7(d). Bearing block 270° location accelerometer spectrum for good roller bearing.

7(e). Bearing block 270° location accelerometer spectrum for roller bearing with inner race defect.

7(f). Bearing block 270° location accelerometer spectrum for roller bearing with rolling element defect.

Figure 7. Wideband acceleration spectra across several test bearing configurations.

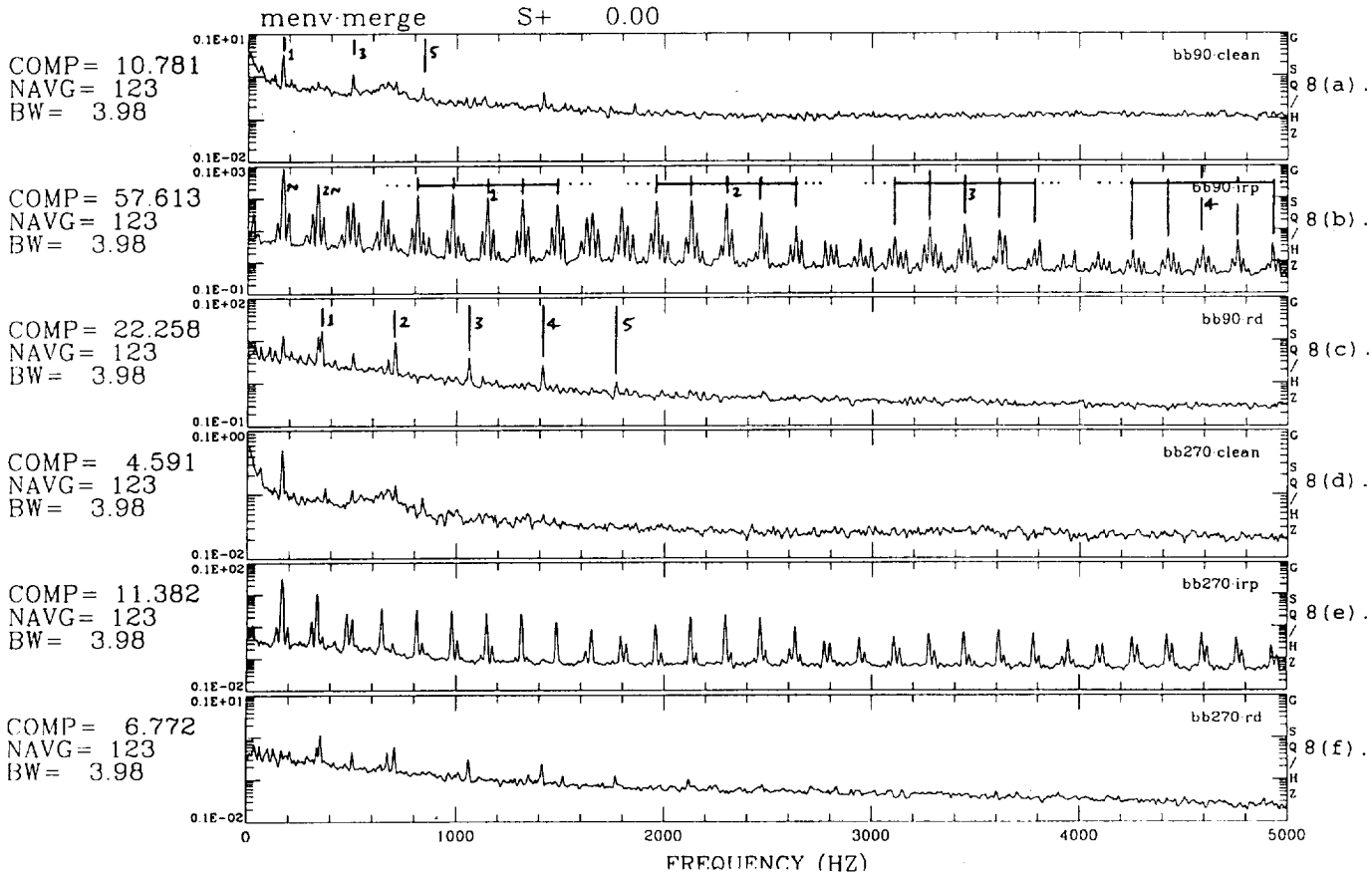

8(a). Bearing block 90° location accelerometer envelope recovered spectrum for good roller bearing.

8(b). Bearing block 90° location accelerometer envelope recovered spectrum for roller bearing with inner race defect.

8(c). Bearing block 90° location accelerometer envelope recovered spectrum for roller bearing with rolling element defect.

8(d). Bearing block 270° location accelerometer envelope recovered spectrum for good roller bearing.

8(e). Bearing block 270° location accelerometer envelope recovered spectrum for roller bearing with inner race defect.

8(f). Bearing block 270° location accelerometer envelope recovered spectrum for roller bearing with rolling element defect.

Figure 8. Envelope spectra derived from wideband acceleration signals across several test bearing configurations.

This allows direct comparison of the spectra of the envelope time signals to their corresponding conventional low-frequency PSD's from the original time signals. As can be seen in the figures, the complexity of the recovered envelope spectra is greatly reduced when compared to the ordinary PSD's of figure 3. This is due in large part to the elimination of the lower-frequency synchronous and broadband noise components. Figures 8(a) and 8(d), which are the recovered envelope spectra from the clean (no implanted fault) bearing test, show spectral peaks at synchronous and a few higher harmonics of synchronous. These spectra are quite different from their corresponding low-frequency PSD estimations seen in figures 3(a) and 3(d) that contain a multitude of discrete components. Figures 8(b) and 8(e) are the spectra recovered from the envelope signals which contain the inner race defect. The similarity of these recovered spectra to the analytically predicted pattern shown in figure 2 is quite impressive. Every peak within the recovered envelope spectra can be linked to the inner race defect/synchronous sideband family structure. Also, note how subsequent harmonics of the inner race roller-passing frequency (IRP), indicated as integers in the figure, exponentially decay as predicted by the analytic model.[4,5] Moreover, both main lobes and side lobes in the synchronous (N) sideband components of each IRP family are apparent and support the analytic predictions as well. With the case of the rolling element defect, as seen in figures 8(c) and 8(f), the analysts were pleased to detect clear evidence of roller spin frequency (RS) and its subsequent harmonics in the envelope data. No substantial evidence of the spin frequency was found using both conventional PSD and nonlinear bispectral analysis of 0- to 5-kHz accelerometer data. Envelope analysis successfully uncovered the subtle roller spin vibration predicted for the seeded defect.

As to why the clean-bearing envelope spectra contain discrete signal content at synchronous and synchronous harmonics (figs. 8(a) and 8(d)), further analysis of similar no-defect roller bearings would have to be performed to verify the recovery as an expected benign indicator.

Figure 9 contains the wideband instantaneous acceleration waveforms which correspond to the envelope recovered spectra of figure 8. The time frame of the sequence coincides with the low-frequency acceleration data shown in figure 4. Unlike the earlier figure, figure 9 depicts the transient ringings initiated by the defective bearing surface impacts occurring during the defect tests. The best examples of this are seen with the wideband acceleration data from the inner race defect test (figs. 9(b) and 9(e)), where successive ringings of the structure are separated by one period of shaft rotation, T_N, or one bearing load cycle. The wideband responses of the roller defect case (figs. 9(c) and 9(f)) are not quite as impressive, and, in fact, are quite similar to the clean (no fault) bearing waveforms of figures 9(a) and 9(d). Regardless of this temporal comparison, spectral analysis of the rolling element defect envelope waveform successfully recovers the bearing fault, distinguishing it from a no-fault bearing.

D. Envelope Detection Analysis Results (Acoustic Emission Data)

In an effort to determine the effectiveness of AE monitoring, the same envelope analysis applied to the wideband accelerometer data was also applied to AE data acquired during each bearing test of the CDDF research. Although, digital signal processing requirements for the AE envelope analysis effort were much more intensive given the envelope bandwidth, 50 to 400 kHz, for the AE's was much higher and broader than that of the accelerometer input, 10 to 80 kHz.

Figure 10 shows the wideband AE spectra across the selected bearing test cases with the envelope analysis bandwidth denoted in figure 10(a). A sensor output calibration error occurred in the recording or reduction of the AE's from the inner race defect case, as can be seen by comparing

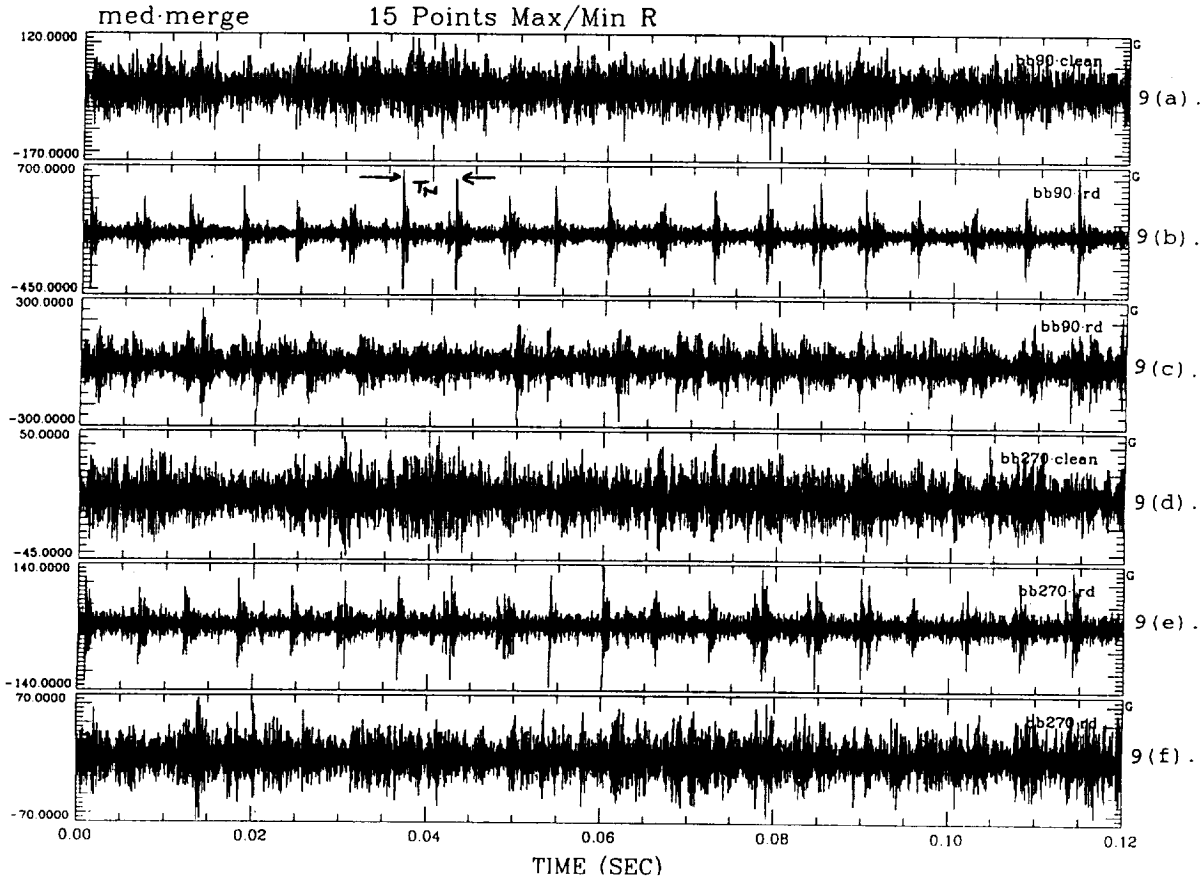

9(a). Bearing block 90° location accelerometer wideband waveform for good roller bearing.

9(b). Bearing block 90° location accelerometer wideband waveform for roller bearing with inner race defect.

9(c). Bearing block 90° location accelerometer wideband waveform for roller bearing with rolling element defect.

9(d). Bearing block 270° location accelerometer wideband waveform for good roller bearing.

9(e). Bearing block 270° location accelerometer wideband waveform for roller bearing with inner race defect.

9(f). Bearing block 270° location accelerometer wideband waveform for roller bearing with rolling element defect.

Figure 9. Wideband acceleration waveforms across several test bearing configurations.

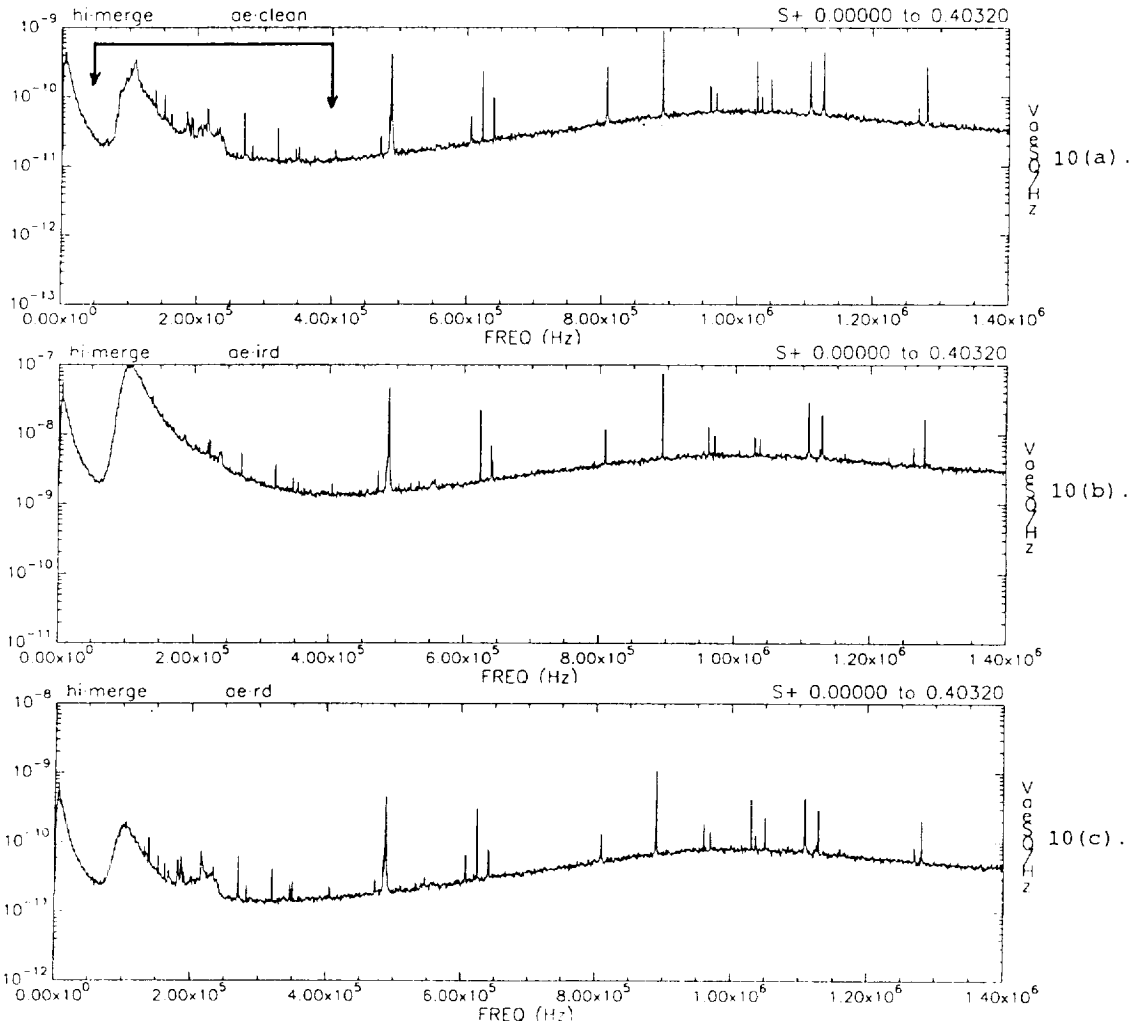

10(a). Wideband acoustic emission spectrum for good roller bearing.

10(b). Wideband acoustic emission spectrum for roller bearing with inner race defect.

10(c). Wideband acoustic emission spectrum for roller bearing with rolling element defect.

Figure 10. Wideband acoustic emission spectra across several test bearing configurations.

the magnitude of figure 10(b) to those of figure 10(a) (clean bearing) and figure 10(c) (roller defect), but the error did not affect the overall results of the envelope recovery process. All three wideband AE spectra are similar in that a majority of the spectral energy is contained in the bandpass region selected for envelope analysis. Figure 11 shows the recovered envelope spectra of the AE's recorded during the selected bearing tests. As with the accelerometer-based envelope spectra, the bearing signatures recovered in the AE envelope spectra are also quite impressive. Figure 11(a) is the envelope spectrum recovered from the AE's recorded during testing of a good roller bearing. The only distinguishable peaks in this spectrum are synchronous (N) related. Figure 11(b) is the AE envelope spectrum from the inner race defect case. As with the accelerometer-sensed envelope spectra, it displays a bearing defect spectrum amazingly similar to analytically predicted model of figure 2. As identified in the figure, families of discrete components with individual members of each

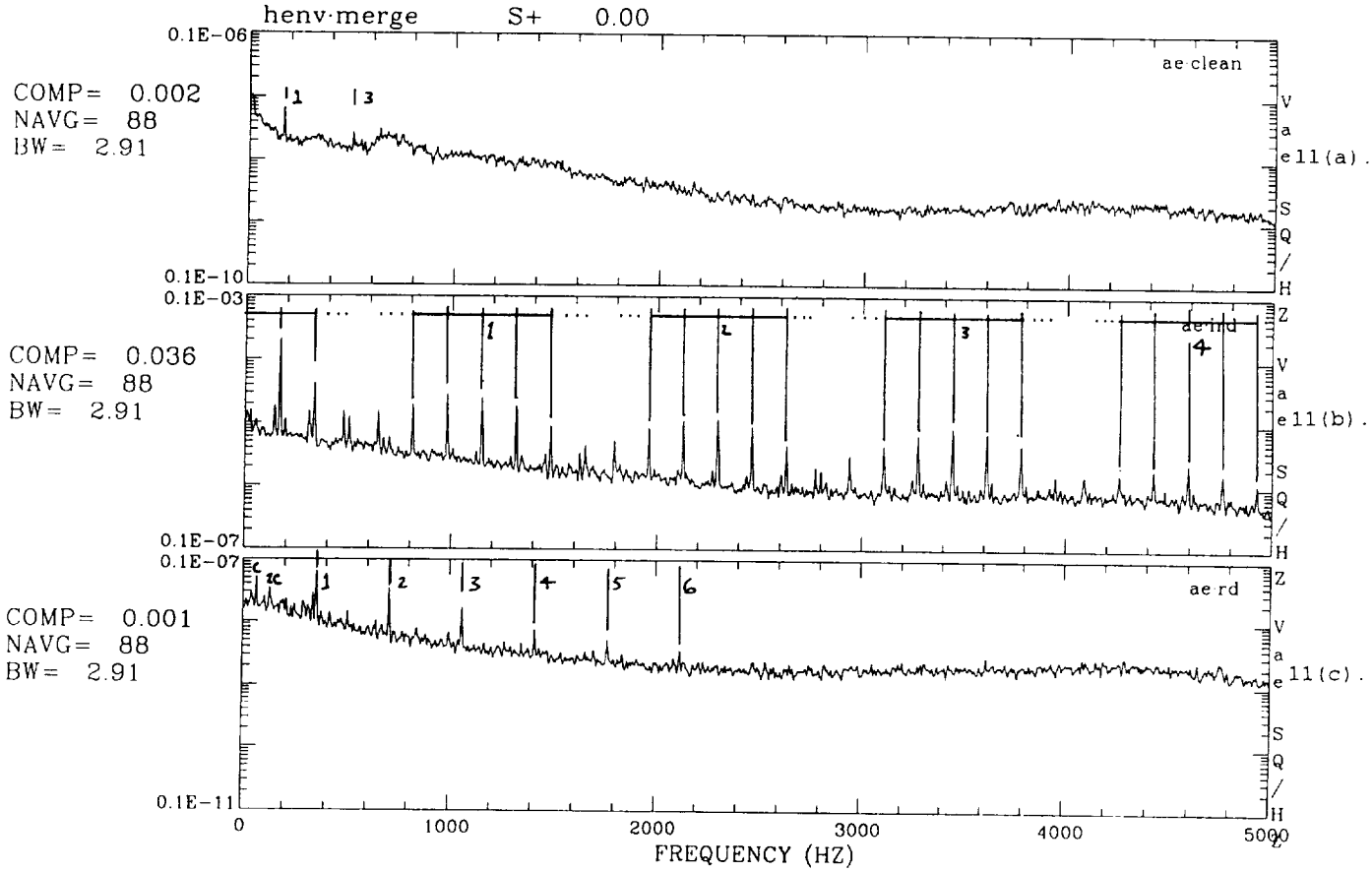

11(a). Acoustic emission envelope recovered spectrum for good roller bearing.

11(b). Acoustic emission envelope recovered spectrum for roller bearing with inner race defect.

11(c). Acoustic emission envelope recovered spectrum for roller bearing with rolling element defect.

Figure 11. Envelope spectra derived from acoustic emissions across several test bearing configurations.

family separated by synchronous frequency are centered about the inner race roller passing frequency (IRP) or its subsequent harmonics. As with the inner race bearing defect signature recovered from the envelope of the wideband accelerometer data, the AE envelope spectrum for the inner race defect case only contains spectral peaks related to the analytically predicted inner race roller passing/ synchronous sideband family signal structure. The AE spectrum also exhibits the characteristic exponential decay in the inner roller-passing frequency chain of harmonics. The spectrum also contains the lobing patterns in the synchronous sideband components of each IRP family (fig. 11(b)). Figure 11(c) is the envelope spectrum recovered from AE's recorded during the rolling element defect test.

As with the successful accelerometer-based envelope recovery of the roller spin defect frequency, AE envelope processing also uncovers the roller spin frequency and subsequent harmonics. In addition, the AE envelope spectrum for the rolling element defect test (fig. 11(c)) contains

evidence of the roller train cage frequency (C) along with its first harmonic (2C). The cage frequency is the analytically predicted modulating frequency for the rolling element defect case as synchronous frequency is for the inner race defect case. Lack of subsequent cage-separated components around roller spin frequency and spin harmonics in figure 11(c) is most likely a result from insufficient side loads being applied to the rotor assembly during testing.

Figure 12 contains the wideband instantaneous AE waveforms that correspond to the recovered envelope spectra of figure 11. These figures relay the highly transient "ringings" initiated by the defective bearing surface impacts, as sensed by the AE sensor during the bearing defect tests. Again, the inner race defect case (fig. 12(b)) shows this transient nature best. In the figure, a series of successive ringings, separated by an interval of approximately one period of shaft rotation, T_N, is very evident. Again, as with the wideband accelerometer characterization, the roller defect case, figure 12(c) is not as impressive, and, in fact, is quite similar to the clean bearing AE waveform of figure 12(a). Regardless, spectral analysis of the roller defect AE envelope (fig. 11(c)) recovers the correct bearing distress indicators (RS and RS harmonics) for the seeded fault.

Figure 13 effectively highlights several key observations made during the research effort. It compares the envelope recovered spectra, from both the accelerometers and AE sensor, to the conventional low-frequency (0- to 5-kHz) acceleration spectrum for the inner race defect case along with the analytically predicted bearing defect vibration spectrum. Peak identification has been purposely omitted in the figure to allow for better overall pattern perception. Figure 13(a) is the conventional 0- to 5-kHz vibration spectrum as sensed by a bearing block accelerometer during the inner race defect test. The ability of envelope detection to "filter out" nonbearing defect-related information is very evident by comparing the basic PSD of figure 13(a) to the envelope spectra of figures 13(b) and 13(c). While figure 13(a) contains bearing defect-related frequency components along with rotor dynamic/structural responses and electronic line noise, all frequencies within the inner roller defect envelope spectra are bearing-defect driven and can be described by the inner roller pass/synchronous sideband modulation pattern predicted in figure 13(d). The intent of this summary-type figure is twofold. First, it delineates the success of envelope analysis (figs. 13(b) and 13(c)) by comparing its results directly to the analytically predicted vibration spectrum for the single-point bearing defect (fig. 13(d)). This correlation was successfully demonstrated using bearing distress signal content contained in radically different frequency bands, i.e., the accelerometer envelope signals were recovered from the 10- to 80-kHz band, while the AE envelope signal was recovered from the 50- to 400-kHz band. This dual success in bearing defect signature recovery through envelope analysis using two totally different sensor technologies, accelerometer and AE, is encouraging in that it identifies multiple analysis paths to the same diagnostic solution. Again, what is of interest in envelope detection-based bearing analysis is not the carrier frequency, which dictates type of sensor, but, rather, the modulating frequency of the carrier or bearing impact repetition rate. Secondly, and more importantly, figure 13 highlights the effectiveness of envelope detection in isolating bearing defect information from extraneous system noise such as rotor dynamic and environmental feedthroughs.

Figure 14 compares the corresponding instantaneous waveforms of the low-frequency (0- to 5-kHz) accelerometer signal (fig. 14(a)), the wideband (10- to 80-kHz) accelerometer signal (fig. 14(b)), and the wideband (50- to 400-kHz) AE's (fig. 14(c)) for the inner race defect test case. While the transient impact events resulting from testing with the imbedded bearing flaw are effectively masked in the low-frequency characterization of figure 13(a), both the wideband accelerometer and AE responses effectively capture them. Figure 14(d) is the instantaneous envelope waveform corresponding to the AE's of figure 14(c). Direct PSD analysis of this envelope waveform resulted in the spectrum of figure 13(c).

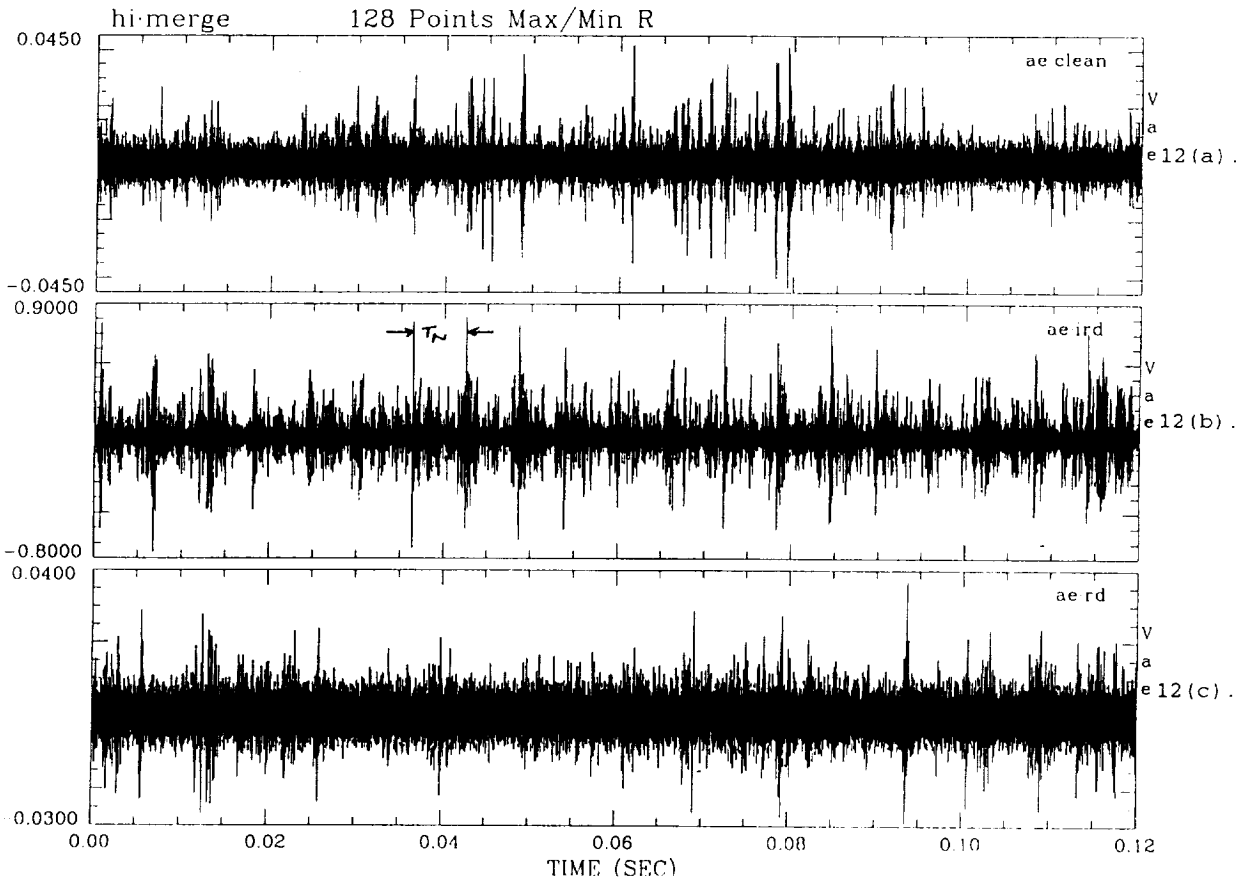

12(a). Acoustic emissions from good roller bearing.

12(b). Acoustic emissions from roller bearing with inner race defect.

12(c). Acoustic emissions from roller bearing with rolling element defect.

Figure 12. Acoustic emission waveforms across several test bearing configurations.

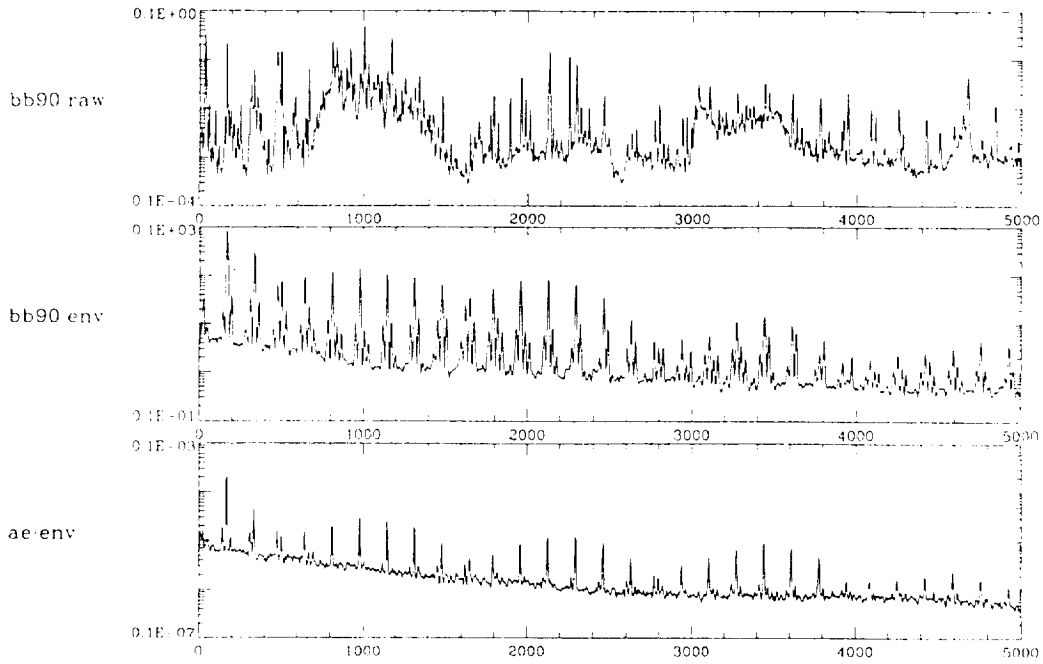

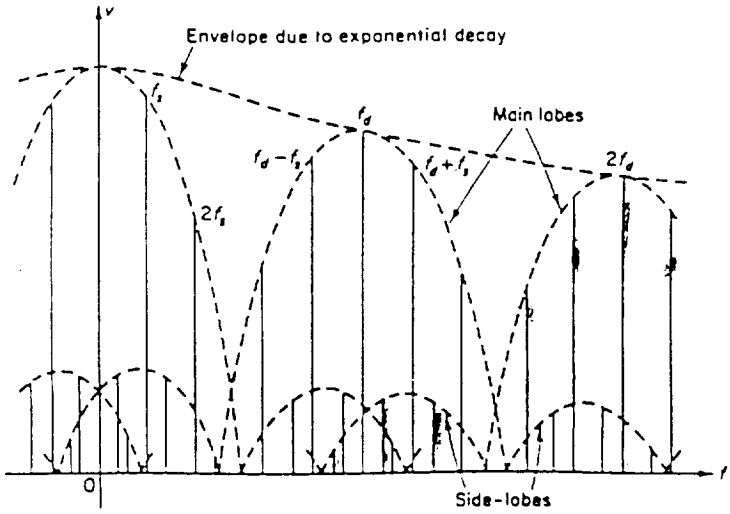

13(a). Bearing block 90° location 0- to 5-kHz acceleration spectrum for roller bearing with inner race defect.

13(b). Bearing block 90° location 0- to 5-kHz envelope recovered spectrum for roller bearing with inner race defect.

13(c). Acoustic emission envelope recovered spectrum for roller bearing with inner race defect.

13(d). Analytically predicted bearing defect vibration spectrum (McFadden and Smith[4]).

Figure 13. Comparison of envelope recovered spectra to conventional vibration PSD and analytically predicted vibration spectrum, roller bearing inner race defect case.

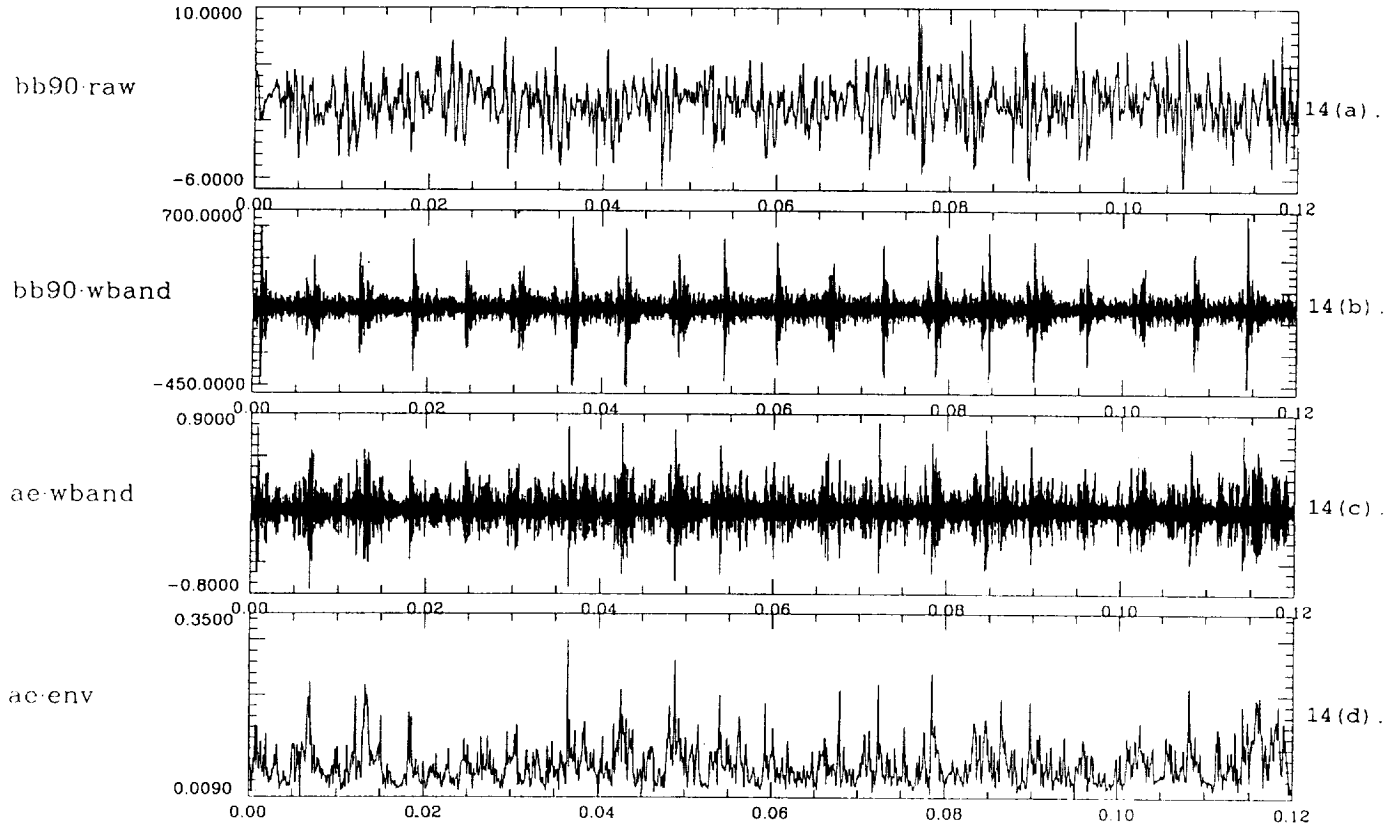

14(a). Bearing block 90° accelerometer low-frequency (0- to 5-kHz) response for roller bearing with inner race defect.

14(b). Bearing block 90° accelerometer wideband (0- to 130-kHz) waveform for roller bearing with inner race defect.

14(c). Acoustic emission response (50 to 400 kHz) for roller bearing with inner race defect.

14(d). Envelope of waveform shown in figure 14(c).

Figure 14. Comparison of wideband and envelope bearing defect waveforms to conventional (0- to 5-kHz) acceleration waveform for inner race defect case.

E. Postenvelope Bispectral Analysis Results

The final leg of this CDDF-sponsored research effort was devoted to the application of nonlinear spectral analysis to the envelope signals of acquired wideband instantaneous acceleration and AE data, i.e., postenvelope bispectral analysis. Given the success of bispectral analysis with conventional low-frequency bearing data (0 to 5 kHz), signal content from the bandwidth where actual characteristic defect frequencies reside, application of nonlinear analysis performed on the envelope of the defect signals, in order to investigate the additional benefits gained, seemed a logical extension of the two technologies.

Figure 15 shows both the bicoherence (fig. 15(b)) and regular PSD (fig. 15(a)) spectra for an accelerometer-sensed wideband envelope time signal from the inner race defect test. Resulting high bicoherence estimates (fig. 15(b)), using a reference frequency set at the inner race roller pass

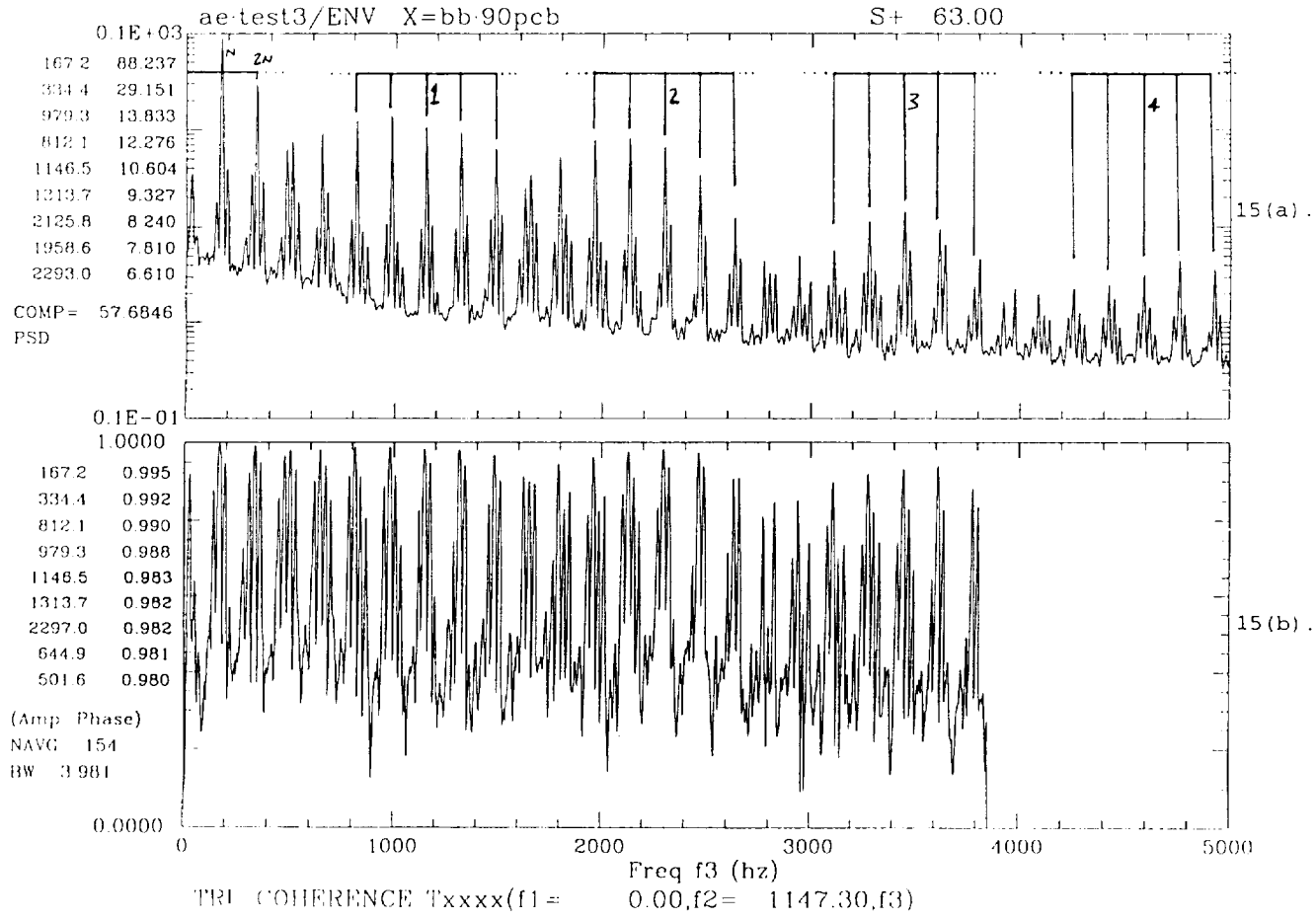

15(a). 0- to 5-kHz PSD of bearing block 90° accelerometer wideband response envelope.

15(b). 0- to 5-kHz bicoherence spectrum corresponding to PSD of figure 15(a), reference frequency set at inner race roller passing impact rate.

Figure 15. Roller bearing inner race defect bicoherence estimation using envelope of bearing block 90° accelerometer data, reference frequency set at inner race roller passing impact rate.

impact rate, not only confirm the harmonic relationship between the inner race passing frequency and its multiples, but also the synchronous sideband (sum and difference) components around the passing frequencies. Figure 16 shows the corresponding bicoherence (fig. 16(b)) and PSD (fig. 16(a)) envelope spectra recovered from the AE transducer recorded during the inner race defect test. Excellent results were obtained with the AE data in that not only the harmonic and sideband signal structure related to the defect was verified, but that superior signal-to-noise ratio in the bicoherence estimate was evident relative to the accelerometer-based estimate shown in figure 15(b). Figures 17 and 18 show similar bicoherence estimations for both accelerometer and AE envelope data, respectively, for the rolling element defect case. As with the inner race defect case, bicoherence analysis using the bearing impact frequency as a reference confirms the harmonic relationship between the fundamental impact frequency and subsequent harmonics.

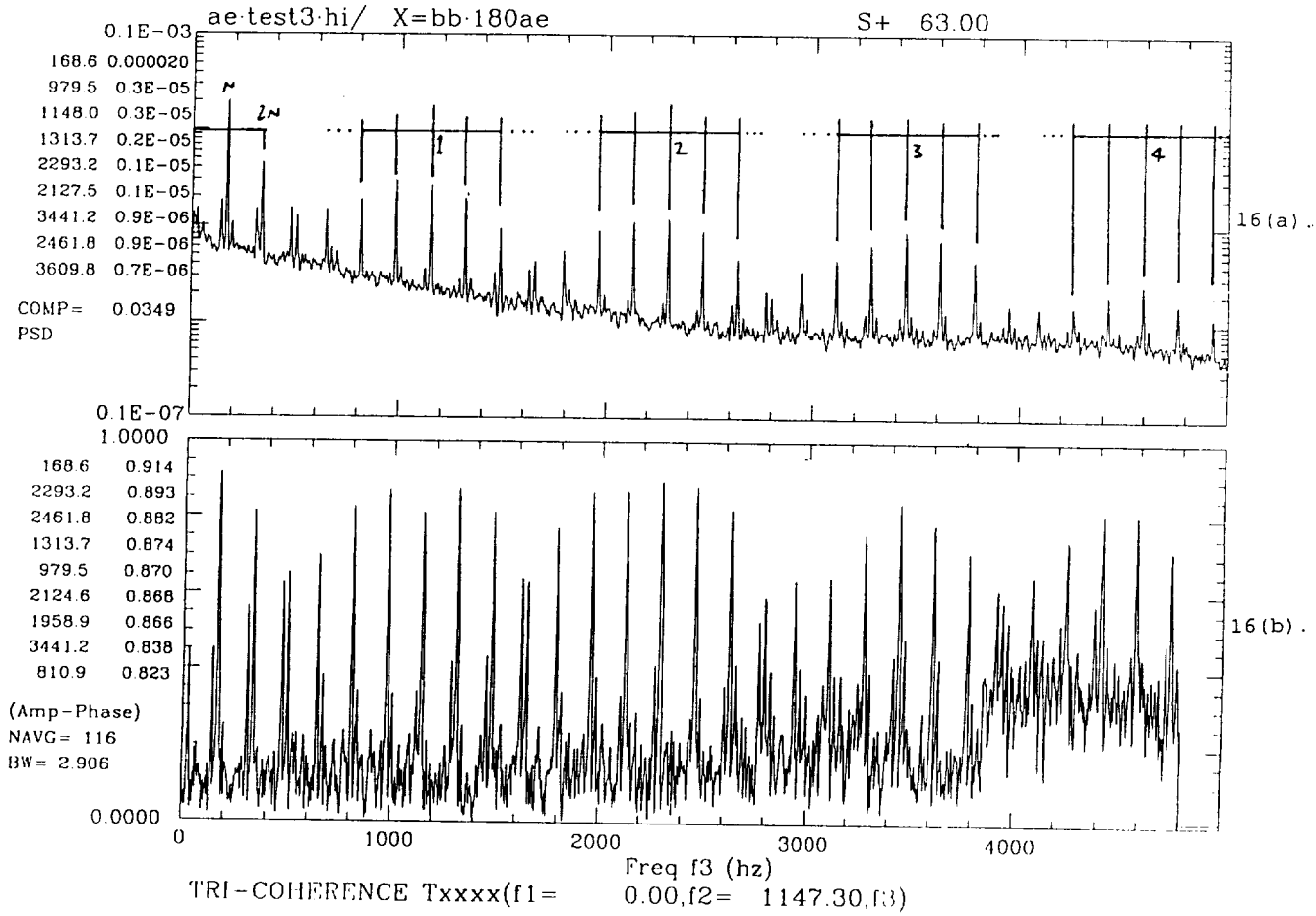

16(a). 0- to 5-kHz PSD of acoustic emission wideband response envelope.

16(b). 0- to 5-kHz bicoherence spectrum corresponding to PSD of figure 16(a), reference frequency set at inner race roller passing impact rate.

Figure 16. Roller bearing inner race defect bicoherence estimation using envelope of acoustic emissions, reference frequency set at inner race roller passing impact rate.

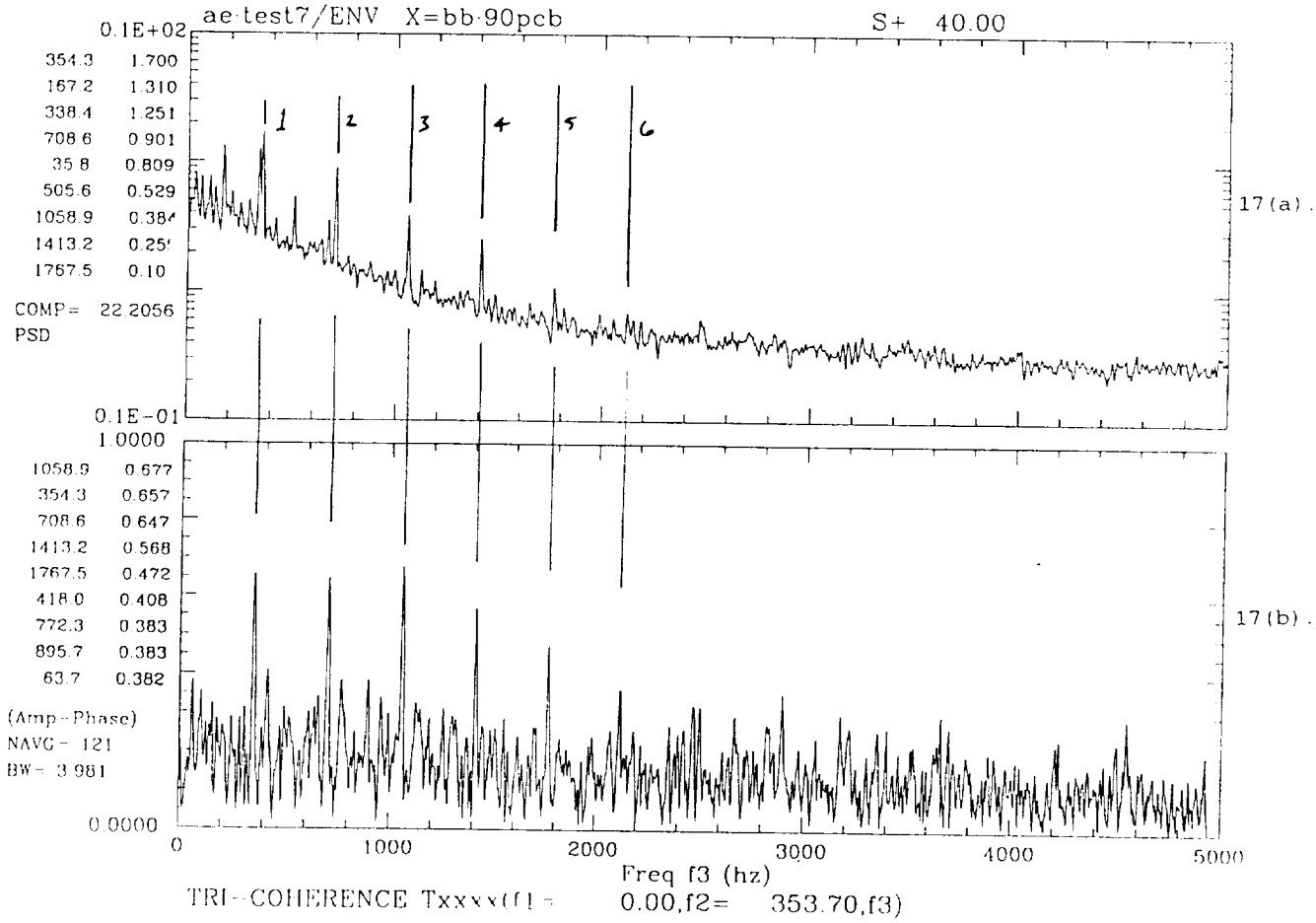

17(a). 0- to 5-kHz PSD of bearing block 90° accelerometer wideband response envelope.

17(b). 0- to 5-kHz bicoherence spectrum corresponding to PSD of figure 17(a), reference frequency set at rolling element spin frequency.

Figure 17. Roller bearing rolling element defect bicoherence estimation using envelope of bearing block 90° accelerometer data, reference frequency set at rolling element spin frequency.

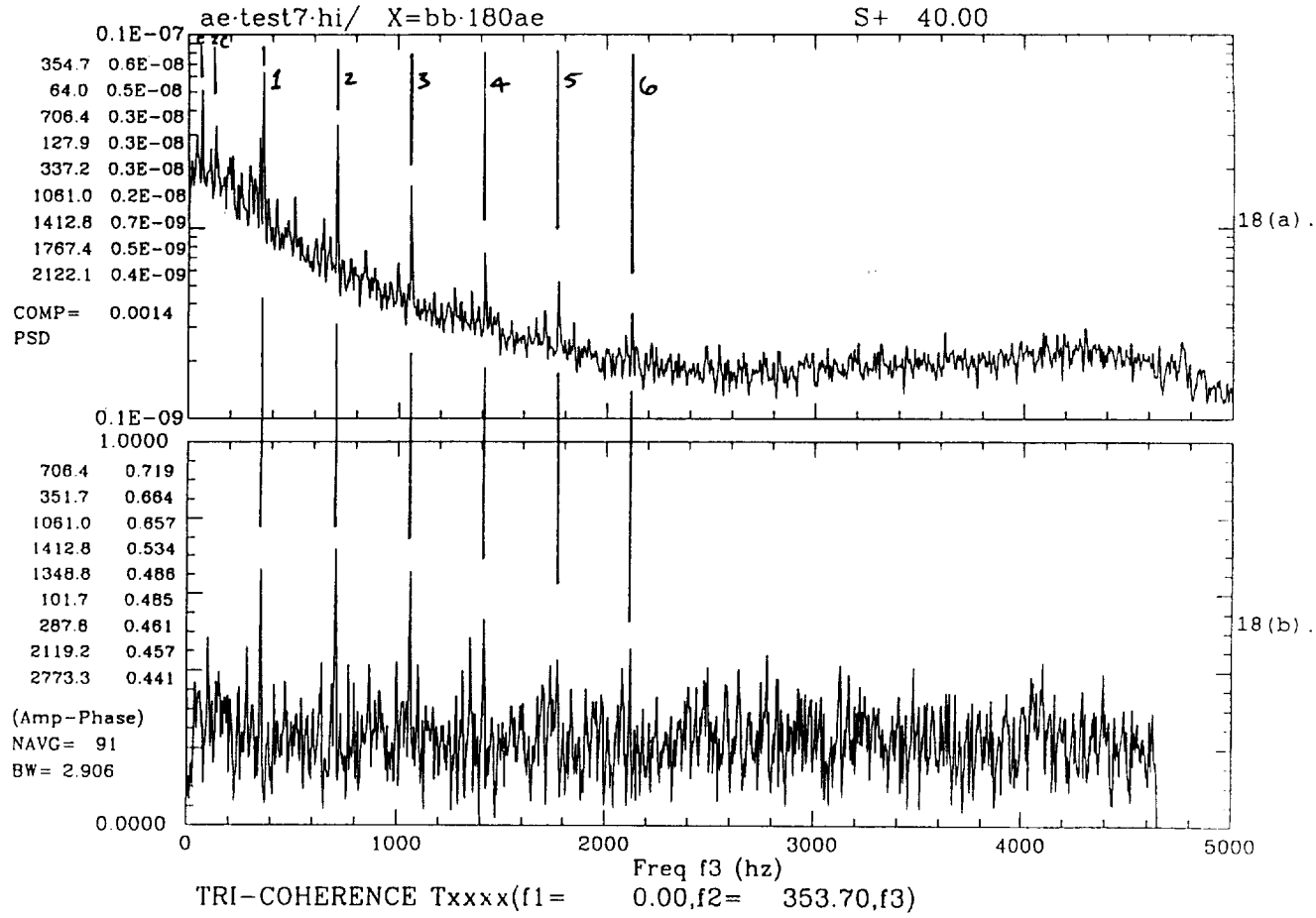

18(a). 0- to 5-kHz PSD of acoustic emission wideband response envelope.

18(b). 0- to 5-kHz bicoherence spectrum corresponding to PSD of figure 18(a), reference frequency set at rolling element spin frequency.

Figure 18. Roller bearing rolling element defect bicoherence estimation using envelope of acoustic emissions, reference frequency set at rolling element spin frequency.

Since the envelope spectra for these single-point bearing defect cases under controlled laboratory conditions have easily recognizable harmonic/modulation sideband patterns in them, applying nonlinear signal analysis to enveloped bearing data may not appear to have added diagnostic value. However, these successful applications prove the concept of coupling the two technologies, thereby laying a foundation for future applications. Future applications will undoubtedly require nonlinear analysis to sort out unidentifiable complex harmonic/modulation sideband patterns resulting from multiple-point defects both within and across heterogeneous bearing sets under complicated operational conditions.

V. SSME TURBOPUMP BEARING EXAMPLE

During developmental testing of the full scale SSME alternate design high pressure oxygen turbopump (ATD HPOTP), one preliminary design of the high speed turbopump consistently experienced extensive pump-end ball bearing wear. The bearing wear developed during hot-fire testing

was typically accompanied by a transient thermal shift in the bearing coolant circuit as registered by the temperature differential across the bearing coolant flow. During the bearing fault investigation efforts, dynamic analysis focused on extracting evidence of pump-end ball bearing distress in high-frequency data channels acquired during SSME hot firings. Conventional low-frequency, 0 to 5 kHz, pump housing acceleration spectra did provide evidence of ball spin (BS) frequencies or its side-bands separated by the ball train cage frequency (C). During the investigation, bispectral analysis of the low-frequency accelerometer data successfully verified several subtle bearing frequencies in the dynamic data.

In an attempt to better characterize the bearing condition during the degradation incidents, envelope analysis of pump-end accelerometer wideband high-frequency data was performed. Figure 19 shows several dynamic indicators just prior to an ATD HPOTP pump-end ball bearing incident that occurred during SSME hot fire 904-159 in December of 1992. Figures 19(a) and 19(b) are 0- to 25-kHz and 0- to 5-kHz pump-end accelerometer PSD's, respectively, reflecting pump housing dynamic response 90 s before a bearing incident. Figure 19(c) is the envelope spectrum generated from the envelope signal recovered from the wideband response, 15-kHz to 25-kHz frequency band, of the pump-end accelerometer. Figure 19(d) is a representative portion of the instantaneous time signal of this wideband waveform used to calculate the envelope spectrum of figure 19(c). During this time frame, there is no evidence of bearing-related frequencies in either the conventional or wideband envelope spectra. The discrete components in the conventional PSD's of figures 19(a) and 19(b) are primarily synchronous (N) or synchronous harmonics due to rotor dynamic and inducer/impeller blade wake responses.

Figure 20 shows the same series of dynamic indicators 90 s later into the hot fire when a significant thermal shift occurred across the pump-end ball bearing coolant circuit. First, notice the increased discrete activity in the 15-kHz to 25-kHz frequency band shown in figure 20(a) as compared to the same PSD taken 100 s earlier, start plus 20 s, shown in figure 19(a). Also, notice the corresponding new subtle peaks in the 0- to 5-kHz band shown in figure 20(b). However, the best dynamic indication of the bearing distress occurring during the thermal shift time frame is shown in the recovered envelope spectrum of figure 20(c). Where the corresponding envelope PSD estimated 90 s prior to the event (fig. 19(c)) shows absolutely no evidence of discrete bearing wear indicators, the envelope spectrum estimated during the event (fig. 20(c)) displays a distinct ball spin (BS) and cage (C) sideband modulation pattern similar to those recovered in this CDDF-sponsored research. Notice the similarity of the recovered SSME ATD HPOTP envelope spectrum to the analytically predicted defect spectrum predicted by McFadden and Smith[4,5] shown in figure 2. The recovered envelope spectrum exhibits not only the characteristic exponential decay in the ball passing frequency (BS) chain of harmonics, but it also exhibits the lobing sideband character attributed to bearing load cycle. Figure 20(d) shows the corresponding wideband acceleration time signal, over approximately 20 shaft revolutions, from which the envelope spectrum was developed. Notice the increase in the peak-to-peak intensity of the waveform as compared to the same indicator taken prior to the bearing event (fig. 19(d)). Bispectral analysis was also applied to the envelope data in an attempt to confirm the modulation sideband pattern related to the bearing damage. Although some degree of nonlinear coupling between spectral peaks in the envelope PSD (fig. 21(a)) was detected, the amplitudes of the bicoherence estimates of the envelope signal using a reference frequency of twice the ball spin (BS) rate (fig. 21(b)) were nowhere near the levels detected in the CDDF test cases (figs. 15(b), 16(b), 17(b), 18(b)). These lower levels of bicoherence for this ATD HPOTP example can most likely be attributed to bearing configuration. Traditionally, nonlinear bicoherence analysis applied to ball-type rolling element bearing defect data yields lesser coherences than those developed from roller-type bearings. However, as shown in figure 21(b), bispectral analysis of the envelope signal is still useful in that it recovers some degree

of nonlinear correlation between the bearing components contained in the corresponding envelope spectrum. Finally, figure 22 shows a time-frequency mapping of the pump-end accelerometer envelope signal over the complete bearing degradation incident hot-fire test. Overlaid on this mapping is the ATD HPOTP pump-end ball bearing coolant flow delta-temperature (discharge minus inlet). As can be seen in the figure, there is an unmistakable correlation between the delta-temperature excursion and recovery of the discrete bearing distress components in the envelope of the wideband acceleration time signal.

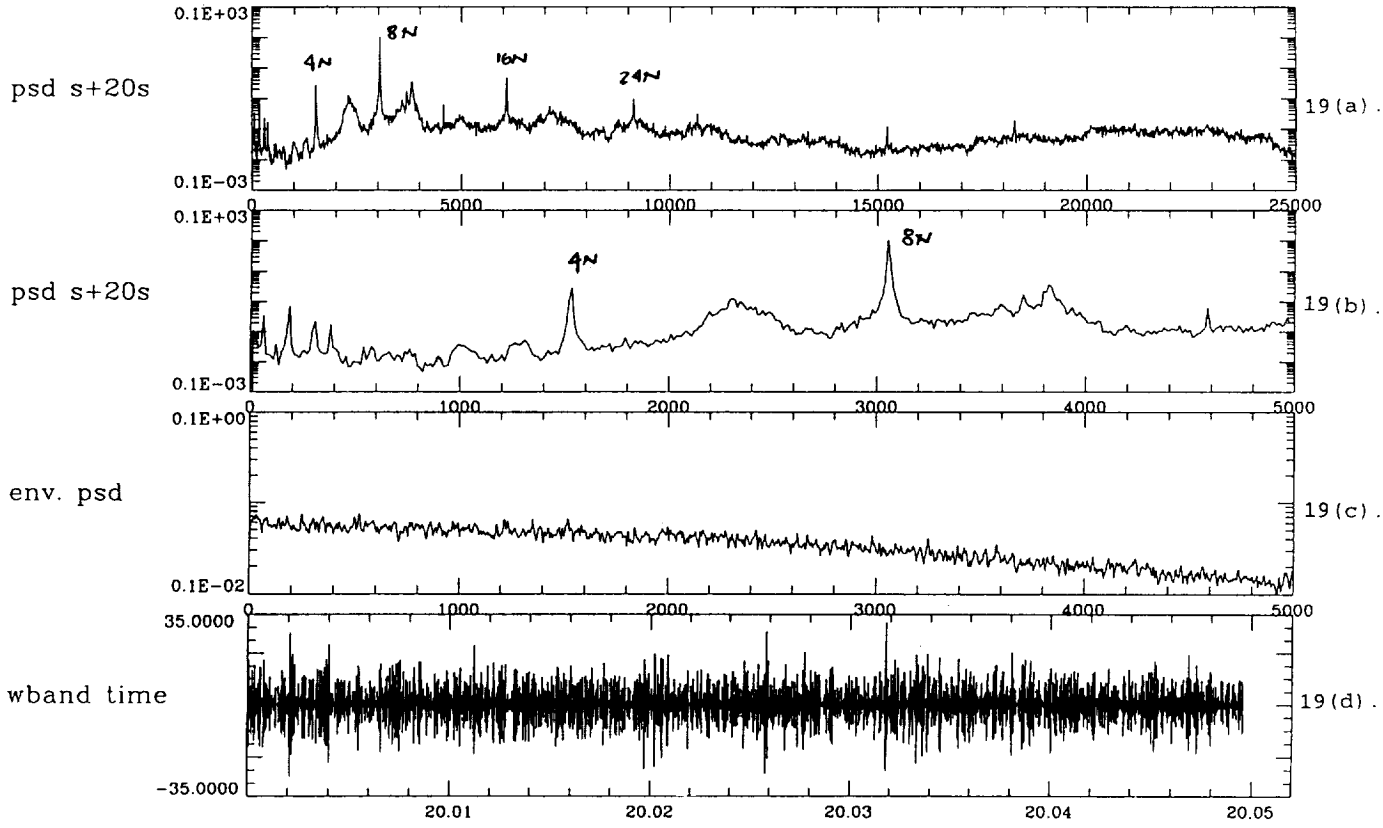

19(a). Pump-end accelerometer 0- to 25-kHz conventional PSD.

19(b). Pump-end accelerometer 0- to 5-kHz conventional PSD.

19(c). Pump-end accelerometer 0- to 5-kHz envelope PSD.

19(d). High-frequency (15- to 25-kHz) waveform from pump-end accelerometer during PSD estimation times of figures 19(a), 19(b), and 19(c).

Figure 19. High-frequency characterization of SSME alternate HPOTP vibration immediately prior to pump-end ball bearing degradation incident.

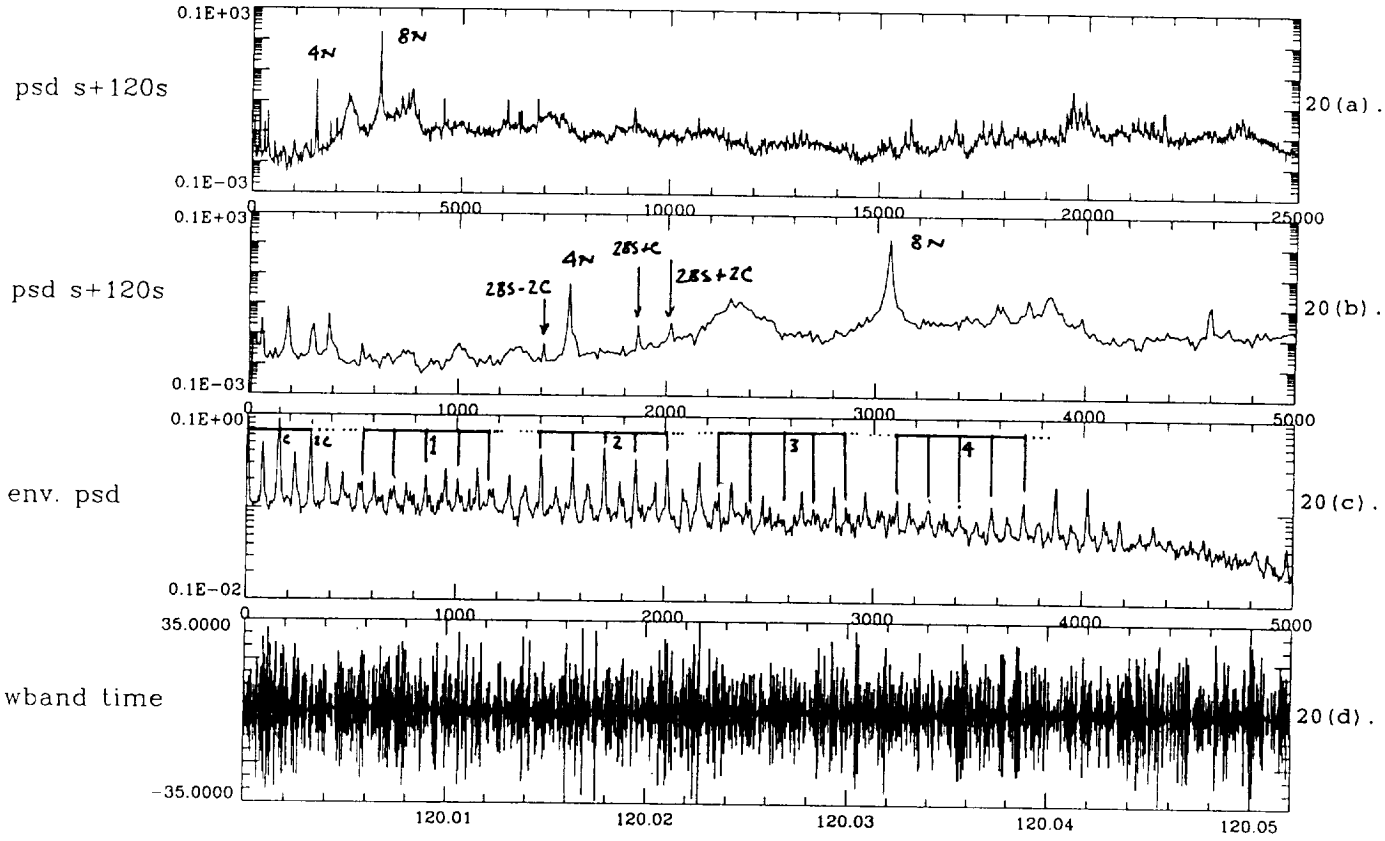

20(a). Pump-end accelerometer 0- to 25-kHz conventional PSD.

20(b). Pump-end accelerometer 0- to 5-kHz conventional PSD.

20(c). Pump-end accelerometer 0- to 5-kHz envelope PSD.

20(d). High-frequency (15- to 25-kHz) waveform from pump-end accelerometer during PSD estimation times of figures 20(a), 20(b), and 20(c).

Figure 20. High-frequency characterization of SSME alternate HPOTP vibration during pump-end ball bearing degradation incident.

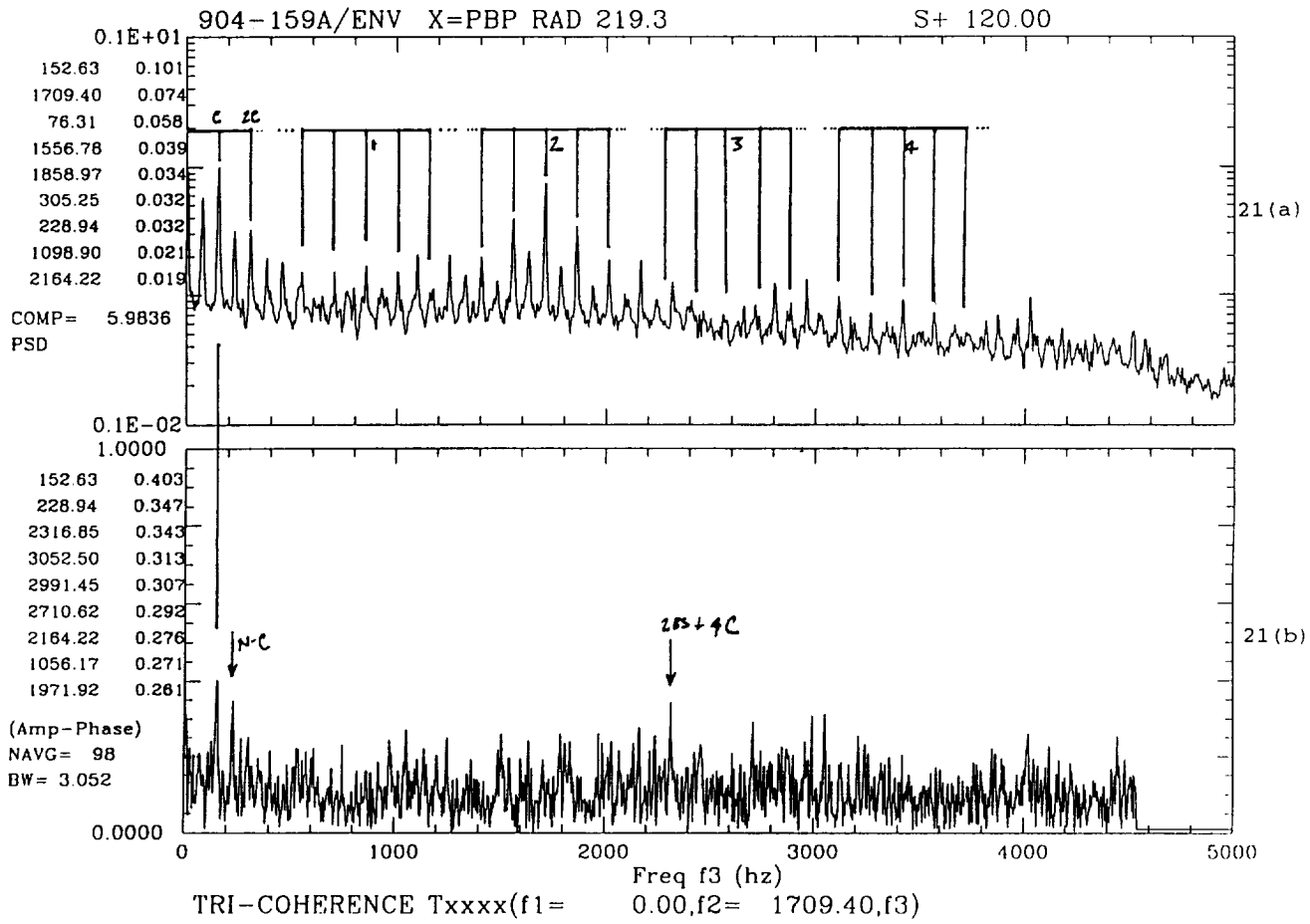

21(a). 0- to 5-kHz PSD of pump-end accelerometer wideband response envelope.

21(b). 0- to 5-kHz bicoherence spectrum corresponding to PSD of 21(a), reference frequency set at pump-end ball bearing ball spin frequency.

Figure 21. ATD HPOTP bicoherence estimation using envelope of wideband pump-end accelerometer data, reference frequency set at pump-end ball bearing ball spin frequency.

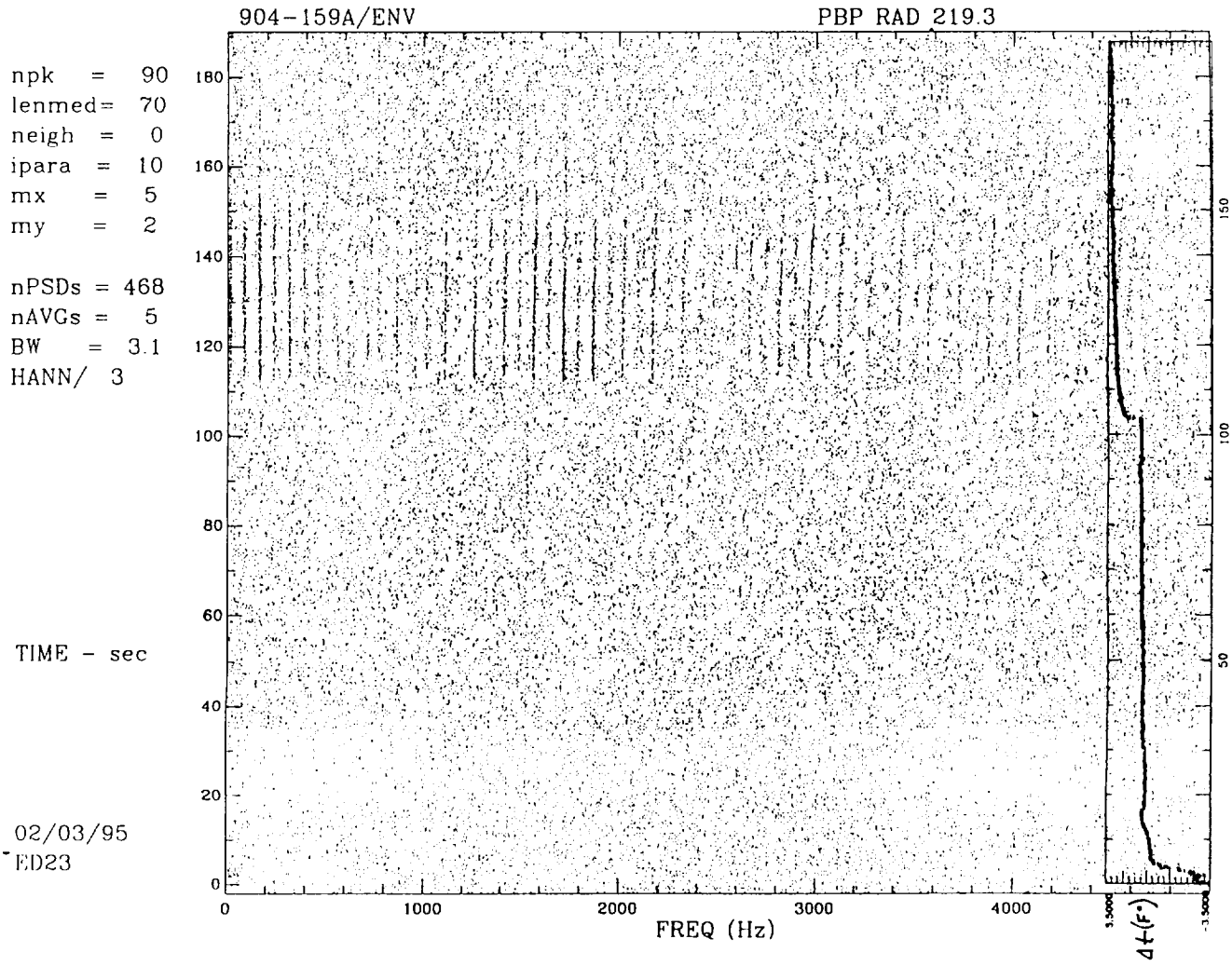

Figure 22. Joint time/frequency mapping of SSME alternate HPOTP pump-end accelerometer recovered envelope signal during pump-end ball bearing degradation incident hot-fire test with ball bearing coolant circuit delta-temperature overlay.

VI. CONCLUSIONS/RECOMMENDATIONS

In summary, this CDDF-sponsored research successfully applied nonlinear signal analysis in the identification of the complex signal structures associated with several single-point bearing defect vibrations. The application was successful using both conventional and AE-type sensor technology. Moreover, bearing defect signatures were identified using both low-frequency, within the band containing the characteristic bearing frequencies themselves, and wideband dynamic data where impacts from seeded bearing defects "rang" structural and sensor resonances. Recovered envelope bearing spectra are strikingly similar to those analytically predicted in literature in that they display symmetric lobing character in sideband structures related to the bearing load cycle. They also consistently show a characteristic exponential decay in the fundamental impact rate harmonic series which is also predicted analytically. This CDDF-sponsored research demonstrated the successful

application of nonlinear bispectral analysis on recovered envelope time signals in identifying complex bearing signatures. Such coupling of technology will undoubtedly be required in future diagnostic evaluations of complex rotating machinery in advanced propulsion systems. Finally, the benefit of AE monitoring for bearing defect analysis was confirmed in the research. In this research, both wideband accelerometer- and AE-sensed responses (signals from two very different frequency regimes) successfully identified seeded test bearing defects. However, in real-world applications, accelerometer-based envelope detection analysis may be unable to recover bearing distress information in complex rotating machinery systems since it is vulnerable to structural noise. In light of this, AE-based envelope detection offers an attractive alternate diagnostic solution.

This accomplished research can be extended in several directions. An in-depth study into bearing defect detection sensitivity thresholds using the diagnostic tools identified in this research, particularly the expanded use of AE technology, would be of great benefit. Research could extend into the characterization of more complex forms of bearing signatures including those from multiple-point defects along with subtle wear patterns such as rolling element-to-element nonuniformities. Also, further application of the diagnostic tools to commercial applications in the transportation, power, and manufacturing industries would undoubtedly prove the techniques' utility.

REFERENCES

1. Harris, T.A.: "Rolling Bearing Analysis." John Wiley and Sons, 1966, pp. 203–207.

2. Tandon, N., and Nakra, B.C.: "Defect Detection in Rolling Element Bearings by Acoustic Emission Method." Journal of Acoustic Emission, vol. 9, No. 1.

3. Holt, J., Palmer, I.G., Glover, A.G., Williams, J.A., and Darlaston, B.J.L.: "Some Examples of Laboratory Application and Assessment of Acoustic Emission in the United Kingdom." Proceedings of the International Institute of Welding Colloquium on Acoustic Emission, 1975, pp. 35–37.

4. McFadden, P.D., and Smith, J.D.: "Model for the Vibration Produced by a Single Point Defect in a Rolling Element Bearing." Journal of Sound and Vibration, vol. 96, 1984, pp. 69–82.

5. McFadden, P.D., and Smith, J.D.: "The Vibration Produced by Multiple Point Defects in a Rolling Element Bearing." Journal of Sound and Vibration, vol. 98, 1985, pp. 263–273.

6. Jong, J., Jones, J., Jones, P., Nesman, T., Zoladz, T., and Coffin, T.: "Nonlinear Correlation Analysis for Rocket Engine Turbomachinery Vibration Diagnostics." 48th Meeting of the Mechanical Failure Prevention Group (MFPG), April 1994.

7. Jong, J., Jones, J., McBride, J., and Coffin, T.: "Some Recent Development in Turbomachinery Fault Detection." NASA 1992 Conference on Advanced Earth-to-Orbit Propulsion Technology, May 1992.

8. Bendat, J.S.: Nonlinear System Analysis and Identification." John Wiley and Sons, 1990.

9. Dugundi, J.: "Envelopes and Pre-Envelopes of Real Waveforms." I.R.E. Transactions on Information Theory, IT-4, No. 1, March 1958, page 53.

APPENDIX

ROLLER BEARING FREQUENCY CALCULATIONS

JEFFCOTT BEARING FREQUENCY CALCULATION–MathCAD file JEFFCOTT BEARING FREQ

Modification for Jeffcott rotor kit SKF roller bearing NU 202 ECP
Dimensions in milli-meters (mm)

$d := 5.5$ $\square$ $\quad dm := 23.8125$ $\quad Nb := 11$

$rad \equiv 1$ $\quad deg \equiv \frac{\pi}{180} \cdot rad$

$\beta i := \beta i \cdot deg$ $\quad \beta o := \beta o \cdot deg$

$\Delta := \beta i - \beta o$

$$BT := \frac{1 - \frac{d}{dm} \cdot \cos(\beta i)}{1 + \cos(\Delta)}$$

$OBP := Nb \cdot BT$

$IBP := Nb \cdot (1 - BT)$

$$BS := \frac{1}{2} \cdot \frac{dm}{d} \cdot \left[1 - \left[\frac{d}{dm} \cdot \cos(\beta i) \right]^2 \right]$$

Contact angles is zero for roller bearings

$\beta i \equiv 0$ $\quad \beta o \equiv 0$

$d \equiv 5.5$

Cage	Outer Ball Pass	Inner Ball Pass	Ball Spin
$BT = 0.385$	$OBP = 4.23$	$IBP = 6.77$	$BS = 2.049$

Cage slip ~0.386

Single row

d 15–20 mm
0.5906–0.7874 in

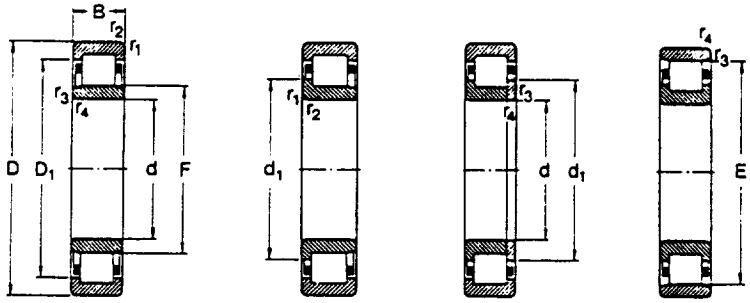

Type NU | Type NJ | Type NUP | Type N

Principal dimensions			Basic load ratings dynamic	static	Fatigue load limit	Speed ratings Lubrication grease	oil	Mass	Designation
d	D	B	C	C_0	P_u				
mm in			N lbf		N lbf	r/min		kg lb	-
15 **0.5906**	35 1.3780	11 0.4331	12 500 2 810	10 200 2 290	1 220 274	18 000	22 000	0.047 0.10	**NU 202 EC**
	35 1.3780	11 0.4331	12 500 2 810	10 200 2 290	1 220 274	18 000	22 000	0.049 0.11	**NJ 202 EC**
	42 1.6535	13 0.5118	19 400 4 360	15 300 3 440	1 860 418	16 000	19 000	0.086 0.19	**NU 302 EC**
	42 1.6535	13 0.5118	19 400 4 360	15 300 3 440	1 860 418	16 000	19 000	0.088 0.19	**NJ 302 EC**
17 **0.6693**	40 1.5748	12 0.4724	17 200 3 870	14 300 3 220	1 730 389	16 000	19 000	0.068 0.15	**NU 203 EC**
	40 1.5748	12 0.4724	17 200 3 870	14 300 3 220	1 730 389	16 000	19 000	0.070 0.15	**NJ 203 EC**
	40 1.5748	12 0.4724	17 200 3 870	14 300 3 220	1 730 389	16 000	19 000	0.073 0.16	**NUP 203 EC**
	40 1.5748	12 0.4724	17 200 3 870	14 300 3 220	1 730 389	16 000	19 000	0.066 0.15	**N 203 EC**
	40 1.5748	16 0.6299	23 800 5 350	21 600 4 860	2 650 596	16 000	19 000	0.092 0.20.	**NU 2203 EC**
	40 1.5748	16 0.6299	23 800 5 350	21 600 4 860	2 650 596	16 000	19 000	0.095 0.21	**NJ 2203 EC**
	40 1.5748	16 0.6299	23 800 5 350	21 600 4 860	2 650 596	16 000	19 000	0.097 0.21	**NUP 2203 EC**
	47 1.8504	14 0.5512	24 600 5 530	20 400 4 590	2 550 573	14 000	17 000	0.12 0.26	**NU 303 EC**
	47 1.8504	14 0.5512	24 600 5 530	20 400 4 590	2 550 573	14 000	17 000	0.12 0.26	**NJ 303 EC**
	47 1.8504	14 0.5512	24 600 5 530	20 400 4 590	2 550 573	14 000	17 000	0.13 0.29	**NUP 303 EC**
	47 1.8504	14 0.5512	24 600 5 530	20 400 4 590	2 550 573	14 000	17 000	0.12 0.26	**N 303 EC**
20 **0.7874**	47 1.8504	14 0.5512	25 100 5 640	22 000 4 950	2 750 618	13 000	16 000	0.11 0.24	**NU 204 EC**
	47 1.8504	14 0.5512	25 100 5 640	22 000 4 950	2 750 618	13 000	16 000	0.11 0.24	**NJ 204 EC**
	47 1.8504	14 0.5512	25 100 5 640	22 000 4 950	2 750 618	13 000	16 000	0.12 0.26	**NUP 204 EC**
	47 1.8504	14 0.5512	25 100 5 640	22 000 4 950	2 750 618	13 000	16 000	0.11 0.24	**N 204 EC**
	47 1.8504	18 0.7087	29 700 6 680	27 500 6 180	3 450 776	13 000	16 000	0.14 0.31	**NU 2204 EC**
	47 1.8504	18 0.7087	29 700 6 680	27 500 6 180	3 450 776	13 000	16 000	0.14 0.31	**NJ 2204 EC**
	52 2.0472	15 0.5906	30 800 6 920	26 000 5 850	3 250 731	12 000	15 000	0.15 0.33	**NU 304 EC**
	52 2.0472	15 0.5906	30 800 6 920	26 000 5 850	3 250 731	12 000	15 000	0.15 0.33	**NJ 304 EC**
	52 2.0472	15 0.5906	30 800 6 920	26 000 5 850	3 250 731	12 000	15 000	0.16 0.35	**NUP 304 EC**
	52 2.0472	15 0.5906	30 800 6 920	26 000 5 850	3 250 731	12 000	15 000	0.15 0.33	**N 304 EC**
	52 2.0472	21 0.8268	41 300 9 290	38 000 8 540	4 800 1 080	11 000	14 000	0.21 0.46	**NU 2304 EC**

APPROVAL

BEARING DEFECT SIGNATURE ANALYSIS USING ADVANCED NONLINEAR SIGNAL ANALYSIS IN A CONTROLLED ENVIRONMENT CDDF FINAL REPORT (NO. 93-10)

By T. Zoladz, E. Earhart, and T. Fiorucci

The information in this report has been reviewed for technical content. Review of any information concerning Department of Defense or nuclear energy activities or programs has been made by the MSFC Security Classification Officer. This report, in its entirety, has been determined to be unclassified.

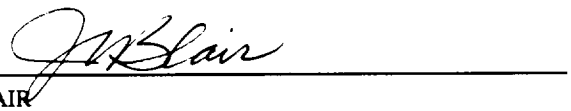

J.C. BLAIR
Director, Structures and Dynamics Laboratory

☆U. S. GOVERNMENT PRINTING OFFICE 1995 633–109 / 20043

REPORT DOCUMENTATION PAGE

Form Approved
OMB No. 0704-0188

1. AGENCY USE ONLY (Leave blank)	2. REPORT DATE	3. REPORT TYPE AND DATES COVERED
	May 1995	Technical Memorandum

4. TITLE AND SUBTITLE
Bearing Defect Signature Analysis Using Advanced Nonlinear Signal Analysis in a Controlled Environment
CDDF Final Report (No. 93-10)

5. FUNDING NUMBERS

6. AUTHOR(S)
T. Zoladz, E. Earhart, and T. Fiorucci

7. PERFORMING ORGANIZATION NAME(S) AND ADDRESS(ES)
George C. Marshall Space Flight Center
Marshall Space Flight Center, Alabama 35812

8. PERFORMING ORGANIZATION REPORT NUMBER

9. SPONSORING/MONITORING AGENCY NAME(S) AND ADDRESS(ES)
National Aeronautics and Space Administration
Washington, DC 20546-0001

10. SPONSORING/MONITORING AGENCY REPORT NUMBER
NASA TM-108491

11. SUPPLEMENTARY NOTES
Prepared by Structures and Dynamics Laboratory, Science and Engineering Directorate.

12a. DISTRIBUTION/AVAILABILITY STATEMENT
Unclassified–Unlimited

12b. DISTRIBUTION CODE

13. ABSTRACT *(Maximum 200 words)*

Utilizing high-frequency data from a highly instrumented rotor assembly, seeded bearing defect signatures are characterized using both conventional linear approaches, such as power spectral density analysis, and recently developed nonlinear techniques such as bicoherence analysis. Traditional low-frequency (less than 20 kHz) analysis and high-frequency envelope analysis of both accelerometer and acoustic emission data are used to recover characteristic bearing distress information buried deeply in acquired data. The successful coupling of newly developed nonlinear signal analysis with recovered wideband envelope data from accelerometers and acoustic emission sensors is the innovative focus of this research.

14. SUBJECT TERMS
bearing diagnostics, nonlinear signal analysis, acoustic emission, turbomachinery health monitoring

15. NUMBER OF PAGES
48

16. PRICE CODE
NTIS

17. SECURITY CLASSIFICATION OF REPORT	18. SECURITY CLASSIFICATION OF THIS PAGE	19. SECURITY CLASSIFICATION OF ABSTRACT	20. LIMITATION OF ABSTRACT
Unclassified	Unclassified	Unclassified	Unlimited